AMELIORATION OF NON-ALCOHOLIC FATTY LIVER DISEASE BY TARGETING GPR110 IN A DIET-INDUCED OBESE MOUSE MODEL

WU MENGYAO

PhD

The Hong Kong Polytechnic University

2023

The Hong Kong Polytechnic University

Department of Health Technology and Informatics

AMELIORATION OF NON-ALCOHOLIC FATTY LIVER DISEASE BY TARGETING GPR110 IN A DIET-INDUCED OBESE MOUSE MODEL

WU Mengyao

A thesis submitted in partial fulfilment of the

requirements for the degree of Doctor of Philosophy

August 2022

CERTIFICATE OF ORIGINALITY

I hereby declare that this thesis is my own work and that, to the best of my knowledge and belief, it reproduces no material previously published or written, nor material that has been accepted for the award of any other degree or diploma, except where due acknowledgement has been made in the text.

(Signed)

WU MENGYAO_   (Name of student)

Abstract

Recent research has shown that the G protein-coupled receptor 110 (GPR110) is an oncogene evidenced by the increased expression of this receptor in numerous cancer types. Cell migration, invasion, and proliferation can all be reduced by GPR110 knockdown. GPR110 is, however, mostly expressed in the liver of healthy individuals. The precise physiological role of hepatic GPR110 in metabolism has not been revealed. In this study, I identified the unique role of GPR110 in association with the liver function in a mouse model of diet-induced obesity using a comprehensive metabolic phenotyping approach.

The expression of GPR110 in the liver was shown to be strictly regulated by nutritional availability using RT-qPCR and Western blot analyses. In both mice and humans, a high hepatic GPR110 level was strongly linked to the probability of developing liver steatosis. The disease severity of mice with non-alcoholic fatty liver disease (NAFLD) induced by a high-fat diet was alleviated when GPR110 was knocked down using antisense oligonucleotides. Stearoyl-coA desaturase 1 (SCD1), a crucial enzyme in hepatic *de novo* lipogenesis, has been identified as a downstream target of GPR110 by RNA-sequencing analysis. Treatment with the liver-specific SCD1 inhibitor MK8245 greatly improved the lipid profiles of GPR110-overexpressing mice and selective shRNAs against SCD1 in GPR110 infected primary hepatocytes

In my thesis work, I hereby provide the first evidence demonstrating that GPR110 plays a physiological role in regulating hepatic lipid metabolism through controlling the expression of SCD1. In obese individuals, down-regulation of GPR110 expression can potentially serve as a protective mechanism to stop the over-accumulation of lipids in the liver. My work has shed light on the future development of a rational therapeutic approach by inhibiting GPR110 for the management of NAFLD.

An abstract of 279 words.

Publications arising from the thesis

Research article

Wu, M., Gani, H., Viney, S., Ho, P., & Orfila, C. (2021). Effect of ginger-enriched pasta on acceptability and satiety. *International Journal of Food Science & Technology*, *56*(9), 4604-4614.

Review

Wu, M., Deng, C., Lo, T. H., Chan, K. Y., Li, X., & Wong, C. M. (2022). Peroxiredoxin, Senescence, and Cancer. *Cells*, *11*(11), 1772.

Deng, C. J., Lo, T. H., Chan, K. Y., Li, X., **Wu, M. Y.**, Xiang, Z., & Wong, C. M. (2022). Role of B Lymphocytes in the Pathogenesis of NAFLD: A 2022 Update. International Journal of Molecular Sciences, 23(20), 12376.

Conference presentation

Wu, M., Deng, C., Lo, T. H., Chan, K. Y., Li, X., & Wong, C. M. (2022). Targeting GPR110 ameliorates non-alcoholic fatty liver disease in diet-induced obese mouse model. Poster presentation. 1st Lipidomics and Decoding Life: From the Technology and Biology Landscapes to Clinical Adaptation.

Patent

US Provisional Patent Application No. 63/370,948 for "Application of GPR110 as target for treating metabolic diseases" [PolyU ref: PAT-1484-US-PSP; SFHF Ref: P24582US00] [EFILEH-SFHC. FID844089]

Acknowledgement

I want to extend my sincere gratitude to Dr. WONG Chi Ming, my major supervisor, for his constant guidance, support, and tolerance throughout my PhD study. Throughout my three years as his PhD student, he is also available to discuss personal issues and future directions, in addition to my project work such as study design and data interpretation. He not only assisted me in finishing my research project but also motivated me to become a professional scientist because of his extensive knowledge and love of education and science. I am grateful to having him as a supervisor, and I had a great time working on his research team.

Furthermore, I am incredibly appreciative of the research team members' assistance. A special thanks goes to Mr. LO TAK HO for helping me with my research. I am also grateful to Miss DENG Chujun and Miss Chan Ka Ying for their assistance in my animal work, and Dr. Yeung Ho Yin Martin for his assistance in my histological study. The support for my experiments from Mr. LI Xiang is also acknowledged.

I would like to express my gratitude to all my friends and coworkers for their assistance and encouragement throughout my PhD studies.

I also want to express my sincere gratitude to the Centralized Animal Facilities team for their assistance with housing and managing my experimental animals, as well as to Dr. Raymond Hui for overseeing departmental lab maintenance and imparting knowledge.

Last but not least, I would like to express my gratitude to my family for their

support, unwavering love, and care throughout my PhD journey.

Table of contents

List of abbreviation

7TM	7-transmembrane structure
ABCA1	ATP binding cassette subfamily A member 1
ACACA	Acetyl-coA carboxylase alpha
ACCA	Acetyl-coA carboxylas
ACOT1	Acyl-coA thioesterase 1
ADGRE1	Adhesion G protein-coupled receptor E1
ADV	Adenovirus
ALT	Alanine aminotransferase
ApoE	Apolipoprotein E
ASO	Antisense oligonucleotide
AST	Aspartate aminotransferase
ATP	Adenosine triphosphate
AUC	Area under curve
BAT	Brown adipose tissue
BCA	Bocinchoinic acid assay
BSA	Bovine serum albumin
CB_1R	Cannabinoid receptor type 1
CD36	Fatty acid translocase
cDNA	Complementary DNA
CHO	Cholesterol
ChREBP	Carbohydrate response element binding protein

CKD	Chronic kidney disease
CVD	Cardiovascular disease
ddH$_2$O	Double-distilled water
DIO	Diet-induced obese
DNA	Deoxyribonucleic acid
DNL	*de novo* lipogenesis
ECD	Extracullar domain
ECL	Enhanced chemiluminescence
ELISA	Enzyme-linked immunosorbent assay
EWAT	Epididymal white tissue
F4/80	Epidermal growth factor-like module containing mucinlike receptor protein 1
FASN	Fatty acid synthase
FBS	Fetal bovine serum
FDA	US food and drug administration
FFA	Free fatty acids
FGF21	Fibroblast growth factor 21
FL	Full length
G-6-P	Glucose-6-phosphate
G6PASE	Glucose 6-phosphatase
GAIN	Autoproteolysis-inducing
GaINAc	N-acetylgalactaosamine

GAPDH	Glyceraldehyde 3-phosphate dehydrogenase
GFP	Green fluorescent protein
GLP-1	Glucagon-like peptide-1
GLUT	Glucose transporter
GPCR	G protein-coupled receptor
GPR110	G-protein coupled receptor 110
GPS	GPCR proteolytic site
GTP	Guanosine-5'-triphosphate
GTT	Glucose tolerance test
H&E	Hematoxylin and eosin
HCC	Hepatocellular carcinoma
HDL	High-density lipoprotein
HFD	High-fat diet
HOMA-IR	Homeostatic model assessment of insulin Resistance
Hspd1	Heat shock protein family D (Hsp60) member 1
i.p.	Intraperitoneal
i.v.	Intravenous
ITT	Insulin tolerance test
kDA	kilodaltons
KEGG	Kyoto encyclopedia of genes and genomes
KO	Knockout

LDL	Low-density lipoprotein
LPL	Lipoprotein lipase
LXR	Liver X receptor
mRNA	Messenger RNA
Mrpl53	Mitochondrial ribosomal protein L53
MUFA	Monounsaturated fatty acids
NAFLD	Non-alcoholic fatty liver disease
NASH	Non-alcoholic steatohepatitis
NC	Negative control
NCD	Non-communicable diseases
NPC	Non-parenchymal cells
ob gene	Obese gene
ORO	Oil Red O
PBS	Phosphate buffered saline
PBST	Phosphate-buffered saline, 0.1% Tween 20
PCR	Polymerase chanin reaction
Pcsk9	Proprotein convertase subtilisin/kexin type 9
Pltp	Phospholipid transfer protein
PTT	Pyruvate tolerance test
PVDF	Polyvinylidene difluoride
qPCR	Quantitative polymerase chain reaction
rAAV	Eecombinant adeno-associated virus

RIPA	Radioimmunoprecipitation assay
RNA	Ribonucleic acid
RT-PCR	Reverse transcription PCR
Rv	Reverse
RXR	Retinoid X receptors
SCD1	Stearoyl-CoA desaturase-1
SDS	Sodium dodecyl sulfate
SDS-PAGE	Sodium dodecyl sulfate polyacrylamide gel electrophoresis
shRNA	short hairpin RNA
SREBP-1c	sterol regulatory element-binding protein 1
STC	Standard chow diet
T2DM	Type 2 diabetes mellitus
TBST	Tris-buffered saline, 0.1% Tween 20
TEMED	Tetramethylethylenediamine
TG	Triglyceride
V	Voltage
VLDL	Very low-density lipoprotein
°C	Degree Celsius
IU	International unit
m	Milli (10^{-3})
μ	Micro (10^{-6})

n	Nano (10^{-9})
p	Pico (10^{-12})
k	Kilo
mol	Mole
M	Molar
l	Liter
g	Gram
mm	Millimeter
μm	Micrometer
h	Hour
min	Minute
sec	Hour
×g	Relative centrifugal force
bp	Base pair
kb	Kilobase pair
kDa	Kilodalton
AU	Arbitrary unit
pfu	Plaque-forming unit

List of figures

List of tables

Chapter 1 - Introduction

1.1 Obesity and non-alcoholic fatty liver disease

1.1.1 Prevalence of obesity and pathogenesis of obesity-related metabolic complications

Despite the urgency of obesity has been addressed since 1980s, the prevalence of obesity is still increasing in the past decades and now becomes a worldwide epidemic (1). It is reported that there are approximately 1.2 billion people were overweight and 300 million people in the world are obesity (2). In 1995, only 10-20% of men and 15-25% of women were obese in Europe, but the percentage increased to 26% and 31% respectively recently (3). On the other hand, the cost of obesity-related health care expenditures in the United State was 24 billion dollars while the amount raised to 75 billion, counting to 5-7% of total health costs in 2003 (4, 5). Except for the United State, Canada, Australia and many Asia countries also under the similar conditions (6-8).

The reason why people is paying more and more attention to obesity is that obesity is the major risk factor for various life-threatening metabolic complications such as type 2 diabetes mellitus (T2DM), non-alcoholic fatty liver disease (NAFLD) and different types of cancer (9-11). A 16-year-cohort study indicated that overweight or obesity was the main predictor of T2DM (12). On the other hand, obesity will lead to a spectrum of liver abnormalities like NAFLD, causing more severe liver disease and a serious cardiometabolic abnormalities (13, 14). According to the World Health

Organization, there are at least 300,000 deaths were due to obesity every year in the United State (1). Therefore, it is great impotent to explore the novel methods to prevent obesity.

1.1.2   Non-alcoholic fatty liver disease

Characterized by an increased intrahepatic triglyceride (IHTG) content with or without inflammation and fibrosis, NAFLD has become an important public health problem because of its high prevalence and the potential progression to severe liver disease like cirrhosis, fibrosis or liver cancer (13). The hallmark of NAFLD is steatosis. Chemically, over the content of 5% or even more of hepatocytes contain visible intracellular triglycerides (TGs) are identified as excessive IHTG or steatosis (15). Obesity, T2DM and hyperlipidemia are coexisting conditions frequently associated with NAFLD. There are 30-100% of obese, 10-75% of T2DM and 20-92% of hyperlipidemia patients suffers from NAFLD (10, 16-19). The prevalence of NAFLD keeps increasing these years, accounting for 10-24% of the population in various countries. NAFLD is the most common cause of abnormal liver-test results among adults in the United States (20). The prevalence of NAFLD is related to many factors such as obesity. With increasing BMI values, the risk of NAFLD also increases. One clinical report showed that the prevalence rates of steatosis and steatohepatitis are approximately 15% and 3% respectively in nonobese person, and 65% and 20% in persons with class I and II obesity (BMI 30.0-39.9 kg/m^2) (21-23).

Apart from obesity, racial and genetic variation also have great influence on NAFLD (24, 25).

1.2 Liver

The liver is a crucial organ that regulates the body's energy metabolism, which is related to metabolism. It connects to many tissues, such as skeletal muscle and adipose tissue, serving as a hub (26). Two thirds of the total cell population in the liver is hepatocytes. The remaining population is nonparenchymal cells such as Kupffer cells and stellate (27). Insulin and other metabolic hormones closely control the metabolic activity. For instance, in the cytoplasm, glucose is converted into pyruvate by the process of glycolysis, and in the mitochondria, pyruvate is totally oxidized to produce ATP (28). Moreover, liver is also the ultimate generator of energy for survive during prolonged caloric deprivation because of its ability to catabolize lipid and amino acids to provide energy for extrahepatic organs (26, 29). Therefore, dysregulation of liver signaling and metabolism is more likely to lead to type 2 diabetes and/or nonalcoholic fatty liver disease (NAFLD).

1.2.1 Liver-extrahepatic tissue crosstalk

Adipose tissue and skeletal muscle are just two examples of the extrahepatic tissues that the liver communicates with closely. Glucose and ketone bodies produced by liver can be delivered to muscle and other tissues, which may

then use them as metabolic fuels when fasting and exercise. Contrarily, muscle supplies the liver with lactate and amino acids, which serve as gluconeogenic substrates for hepatocytes to synthesize glucose (30). When fasting and exercise, adipose tissues lipolyze to create NEFAs and glycerol (31). Thereafter, the fatty acids were either packaged into VLDL particles or oxidized to produce ketone bodies (32). After that, the liver secretes ketone bodies and VLDL, which extrahepatic tissues use. Hepatocytes further employ glycerol for the production of glucose or TG.

1.2.2   Glucose metabolism

Liver is the organ that response to the nutrient status and it is responsible for glucose clearance. For this reasons, insulin resistance in liver is the major contributor to glucose intolerance and hyperglycemia in obesity (33). A plasma membrane glucose transporter by the name of GLUT2 allows blood glucose to enter hepatocytes. Hepatocytes' ability to absorb glucose is impaired when GLUT2 is inhibited (34). A reduction in intracellular glucose concentrations and an increase in glucose uptake may result from the phosphorylation of glucose by the enzyme glucokinase in the hepatocytes (35). Additionally, G6P undergoes glycolysis as part of its metabolism to produce pyruvate. The tricarboxylic acid (TCA) cycle is used to completely oxidize pyruvate within the mitochondria, producing ATP (36). On the other hand, pyruvate can also be used in lipogenesis to create fatty acids (37). The pentose phosphate pathway is also used to metabolize G6P to produce

NADPH, which is necessary for lipogenesis and the production of other bioactive chemicals (38). Collectively, During the postprandial stage, glucose is transformed into glycogen, fatty acids, or amino acids in the liver.

Glycogen phosphorylase hydrolyzes glycogen during fasting to produce glucose (glycogenolysis). Glycogen synthase, in addition to posttranslational changes, is regulated by glycogen synthase kinase 3 (GSK-3), which limits the activity of glycogen synthase (39). Additionally, the main mechanisms that trigger the activation of gluconeogenic enzymes in the liver are glycerol from lipolysis of white adipose tissue (WAT), pyruvate produced from glycogenolysis, and glycolysis in skeletal muscle (39, 40). Other investigations revealed that phosphoenolpyruvate carboxykinase (PEPCK) controls the conversion of cytoplasmic oxaloacetate, which is produced from pyruvate, to phosphoenolpyruvate, making it a crucial enzyme for gluconeogenesis. However, animals with liver-specific PEPCK depletion maintained their normal 24-hour fasting blood glucose levels, indicating that glycerol might be a more significant substrate for gluconeogenesis (41, 42).

1.2.3 Lipid metabolism

When the body has enough carbohydrates, the liver will not only use glucose as the primary metabolic fuel but also transform it into fatty acids (43). Fatty acids from diet or secreted from adipose tissue can be taken up by hepatocytes from the circulation. Following a meal, enterocytes in the small intestine are primarily responsible for digesting dietary fat. Here, fatty acids

6

are reprocessed into TAG and released into the gut lymphatic system in the form of chylomicrons (44). Chylomicrons pass through the bloodstream to the liver, where they undergo lipolysis and release NEFAs through the action of lipoprotein lipase (LPL). NEFAs then enter into hepatocytes by CD36 in hepatocytes, leading to an increased hepatocyte fatty acid uptake and TG levels (45). On the other hand, liver is able to convert carbohydrates into fatty acids, which are consequently packed into VLDL particles and delivered to adipose tissue or other extrahepatic tissues through the bloodstream through *de novo* lipogenesis. Pyruvate is imported into the mitochondria and metabolized to generate acetyl-CoA, which is combined with oxaloacetate to form citrate. Citrate is then exported to the cytoplasm Acetyl-CoA carboxylase (ACC) converts acetyl-CoA into malonyl-CoA in the cytoplasm. Fatty acid synthase (FAS) uses both malonyl-CoA and NADPH as precursors to create palmitic acid, a fatty acid with 16 carbons (46). Fatty acyl-CoA elongase (Elovl) family members extend palmitic acid (47). Long-chain fatty acids are desaturated by stearoyl-CoA desaturases (SCDs) for the formation of mono- and poly-unsaturated fatty acids (48). It is reported that global knockout of SCD1, which catalyzes the synthesis of monounsaturated long-chain fatty acids can protect against obesity (49, 50). Additionally, hepatocyte-specific SCD1 deletion can prevent from hepatic steatosis and obesity (51). SCD1 products, particularly oleate, are now playing an increasingly significant role in regulating lipid and glucose metabolism in the liver (51).

The progression of lipogenesis is regulated by a large number of transcriptional factors and coregulators such as PPARγ. The expression of PPARγ is low at normal level in mice, and the level is increased in mice with obesity (52). It is known that hepatic PPARγ regulates many genes which control fatty acid uptake, fatty acid trafficking and TG biosynthesis in liver (53, 54). Hepatic specific knockdown of PPARγ suppresses the expression of many lipogenic genes and therefore protect against hepatic steatosis (55, 56). Another study demonstrated that CREB suppresses PPARγ by stimulating the expression of hairy enhancer of split (HES-1) (57) while a separate research reported that the knockdown of CREB in liver can decrease the hepatic lipogenesis in rodents with type 2 diabetes (58).
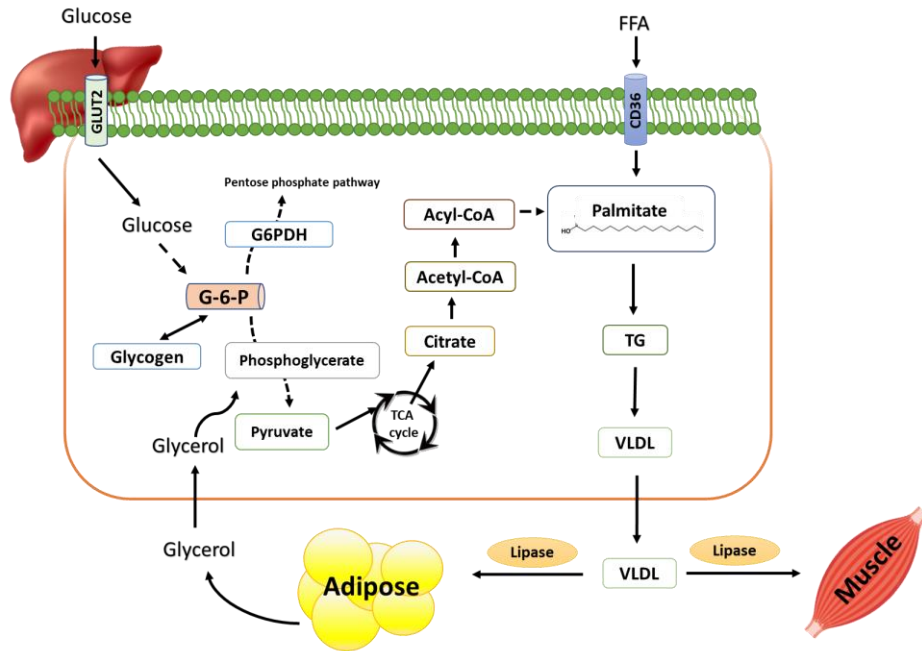
Figure 1.1 Glucose and lipid metabolism in liver. The simplified metabolic pathways of hepatic glucose and lipid.

1.3   GPCR

1.3.1   General introduction

At least 800 different members comprise the G protein-coupled receptor
(GPCR) superfamily, which all share a highly conserved 7-transmembrane
(7TM) structure that converts extracellular stimuli into intracellular
signaling cascades. Each GPCR expresses independently and responds to a
specific ligand with unique specificity. Specific stimuli, such as light protons,
ions, odorants, and biological ligands, can activate these receptors (59). The
conserved structure of GPCRs is made up of seven TMD of roughly 25–35
amino acid residues. These TMD exhibit relatively high levels of
hydrophobicity, and they are identified by a-helices that cross the plasma
membrane (60). The GPCR family is divided into five subfamilies using
phylogenetic analysis, with the rhodopsin or class A family being the biggest
with over 700 members (61). Peptide-binding receptors, which include
secretin and adhesion receptors, belong to the class B GPCRs. It has been
proposed that all Class B ligands are peptide hormones that have a high
degree of homology with one another, making them suitable therapeutic
targets for neuronal and endocrine disorders (62).

1.3.2   Structure of class B GPCR

In comparison to other GPCRs, Class B GPCRs have very high molecular
weights due to their distinctive, extraordinarily lengthy extracellular regions
at the N-terminal of the 7TM domain. The extracellular domain (ECD) of

the receptor contains repetitions of N-linked glycosylation sites (63). The GPCR autoproteolysisinducing (GAIN) domain, which has a self-cleavage site known as the GPCR proteolytic site (GPS) (64), connects the ECD and 7TM domains. An approach for activating class B GPCRs is provided by previous in vivo and in vitro studies that shown that monoclonal antibodies directed against the N-terminal of GPCRs can imitate the role of agonist in increasing downstream activity (65). Recent studies have demonstrated that class B GPCRs may be triggered by their own tethered agonist, specifically -strand-13, upon self-cleavage at the GAIN domain (64, 66). Class B receptors share the same basic structure, which consists of seven membrane-spanning α-helices linked by a G protein-interacting intracellular domain. Class B receptors have a large extracellular domain (ECD; 1 to 16 residues) at the N-terminus that is essential for ligand binding (59). Conserved cysteine residues can be found in the first and second extracellular loops of the TMD sections of these receptors. A significant portion of the receptors in this family do, however, have conserved cysteine residues, which when combined create a group of cysteine bridges in the N-terminus. The secretin receptors' three binding domain names area, juxta-membrane region of the N-terminus, and extracellular loops — define the binding profile of these receptors. These extracellular loops boost the likelihood that the signaling units will activate by mediating the receptor's active conformation (60).

1.3.3   Signal transduction of GPCR

The largest superfamily of cell-surface receptors involved in TMD signaling is the GPCR family. GPCRs typically transmit signals into cells as a result of their reactions to various extracellular stimuli, such as ions, polypeptides, and glycoproteins, and then they regulate a wide range of physiological and developmental function. Class B GPCR signaling is carried out by both G protein-dependent and independent mechanisms. The intracellular C-terminal of the receptor is bound by heterotrimeric G proteins in the traditional G protein-dependent pathway, which mediates the downstream cascade (67). A complex of GTP-bound Gα, Gβ, and Gγ subunits makes up the heterotrimeric G protein structure. When an external stimulus is present, GTP binding causes the Gα subunit to dissociate. As a result, the Gα subunit and G$\beta\gamma$ complex will communicate with the corresponding downstream effector proteins. GTP is hydrolyzed to GDP to end the signal (67). In this context, the subtype of the Gα subunit, which includes Gαs, Gαq, Gαi, and G12/13, determines the downstream effector to be activated. Gαs and Gαi are counter regulators of the PKA pathway through activation and inhibition of adenylate cyclase activity, respectively [163, 164]. The C-terminal of GPCRs is connected to β-arrestin in a G protein-independent route, which facilitates internalization of the receptor or activation of kinase signaling networks (68). Arrestins were first described as proteins that turn off G protein signaling phosphorylation of the receptor C-terminal tail by a G protein-linked kinase leads to recruitment of arrestin, which prevents

12

interaction with G proteins and promotes receptor internalization. However, certain GPCR ligands can activate arrestin binding directly or possibly by promoting interaction with kinases that phosphorylate the receptor to enable arrestin binding, thereby activating downstream signaling pathways distinct from those mediated by G proteins (69) (Fig. 1.2).
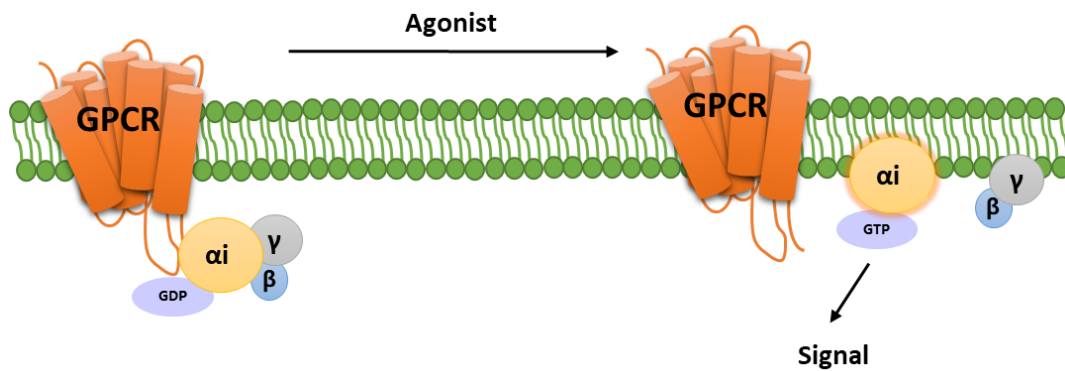
Figure 1.2. Signal transduction of GPCRs. The heterotrimeric G protein structure is a complex of GTP-bound Gα, Gβ, and G γ subunits. Briefly, GTP binding can lead to Gα subunit dissociation and interaction with the effector. Hydrolysis of GTP to GDP will terminate the signal transduction. Different subtype of Gα subunit has different effector for downstream signaling transduction.

1.3.4 Physiological roles of class B GPCRs in metabolism

A class B GPCR's physiological role is mostly determined by the ligand that interacts with the relevant extracellular domains (70). The first-class B GPCR to be discovered was mucin-like receptor protein 1 (F4/80), which is found in the epidermal growth factor-like module (71). It is a well-established pro-inflammatory signal in metabolically active tissues including the liver and adipose tissue and plays a crucial role in the activation of regulatory T-cells in peripheral tolerance (72). Class B GPCRs also have significant regulatory functions in the metabolism of energy. For instance, one of the important regulators that triggers glycogenolysis and gluconeogenesis during fasting situations is the glucagon receptor in the liver (73). For instance, one of the important regulators that triggers glycogenolysis and gluconeogenesis during fasting situations is the glucagon receptor in the liver (73). GLP-1 activation can boost insulin production from -cells and reduce appetite via acting on the brain because GLP-1 receptors are present in the pancreas, gut, and brain (74). Dysregulation of GPCRs is also linked to the emergence of cancer (75).

1.3.5 Class B GPCR as potential drug targets for metabolism diseases

GPCRs are important targets for translational therapy because of their physiological importance (76). GPCRs are the most often used class of drug targets when compared to other approved treatment techniques, according to

research that 36% of US Food and Drug Administration (FDA)-approved medications in 2017 target GPCRs (76). However, current drug development programmes mainly focus on small sector of the potentially druggable human GPCRs, while many orphan GPCRs remained understudied (68). Therefore, it is crucial to research the physiological roles played by orphan GPCRs in order to overcome obstacles in the search for medicines that can treat metabolic illnesses.

1.3.6   GPR110

In 2002, the highly conserved amino acid sequences of the G protein coupled receptor transmembrane domains allowed for the identification of the human GPR110. Two years later, the same research team discovered the mouse ortholog of hGPR110 (77), and extensive sequencing analyses found several splice variants (78). Most research on GPR110 to date has been on how tumorigenic it is. GPR110 was often found to be overexpressed in a variety of malignancies and was necessary for promoting cancer cell survival, proliferation, and migration. As a result, it was proposed that GPR110 targeting could be a novel therapeutic approach for the management of cancer. Additionally, GPR110 was said to be necessary for healthy fetal brain development and the reduction of neuroinflammation [14]. GPR110 is, however, mostly expressed in adult livers (79). GPR110 is, however, mostly expressed in adult livers. The hepatic GPR110's physiological role is still

unknown. In this investigation, using a diet-induced obese mice model, we evaluated the metabolic effect of GPR110 in promoting hepatic lipid buildup.

1.4 General aims of this study

Obesity is a major contributor to multiple chronic metabolic diseases, such as NAFLD. Recent studies have provided insights into the dysregulation of hepatokines and GPCRs leads to the pathogenesis of metabolic diseases and accelerating cancer development. In this thesis, our team demonstrating the G protein-coupled receptor 110 (GPR110) – an orphan class B GPCR exclusively expressed in the liver, are markedly downregulated after high-fat diet (HFD) treatment. The major objective of this study was therefore to investigate the physiological roles of GPR110 in the progression of NAFLD.

In this study, the physiological roles of a novel GPCR were characterized in Chapter 3. We have demonstrated that hepatic GPR110 is tightly regulated by nutrient availability and remarkably reduced in the DIO mice model. Restoration of GPR110 expression by recombinant adenoassociated virus (rAAV) mediated gene delivery in DIO mice accelerates the progression of NAFLD with significantly increasing their body weight and increased circulating and hepatic lipid deposition. The molecular mechanism whereby GPR110 regulates lipid metabolism is further investigated. We demonstrated that GPR110 targeted knockdown using antisense oligonucleotides (ASOs) reverses all the metabolic phenotyping changes. These findings assessed the

metabolic impact of GPR110 in enhancing liver lipid accumulation by diet-induced obese mouse model.

In Chapter 4, we demonstrated that SCD1 is one of the downstream targets of GPR110 that affecting hepatic lipid metabolism. SCD1 is a crucial lipogenic enzyme that forms double bonds in saturated fatty acids to complete the rate-limiting step in the production of monounsaturated fatty acids (MUFAs), such as oleate and palmitoleate (80). Increases in SCD1 activity play a role in the development of NAFLD, hypertriglyceridemia, atherosclerosis, and diabetes (81, 82), all of which are lipid disorders. MUFAs are the building blocks for the synthesis of many different types of lipids. *In vitro* assays were performed to confirmed that the transcription level of SCD1 is regulated by GPR110. We also examine the up regulation of hepatic SCD1 is the cause of metabolic dysregulation in rAAV-GRP110 mice. Furthermore, therapy of MK8245, one of the known SCD1 inhibitor, improves lipid profiles and reduce metabolic dysregulation led by hepatic GPR110 overexpression in mice. The overall significance of the findings and potential future work are discussed in Chapter 5.

Chapter 2 - Materials and methods

2.1   Material

2.1.1   Chemicals and reagents

Reagents	Provider	Catalog number
Dulbecco's modified eagle medium, powder, high glucose, pyruvate	Thermofisher, USA	12800082
Fetal Bovine Serum, qualified, Brazil	Thermofisher, USA	10270106
Penicillin-Streptomycin (10,000 U/mL)	Thermofisher, USA	15140163
TRIzol™ Reagent	Thermofisher, USA	15596018
PageRuler™ Plus Prestained Protein Ladder, 10 to 250 kDa	Thermofisher, USA	26620
TEMED	Thermofisher, USA	17919
Collagenase, Type II, powder	Thermofisher, USA	17101015
Ethidium Bromide Solution	Thermofisher, USA	17898
SYBR™ Safe DNA Gel Stain	Thermofisher, USA	S33102
Mitochondria Isolation Kit for Cultured Cells	Thermofisher, USA	89874
Richard-Allan Scientific™ Neutral Buffered Formalin (10%)	Thermofisher, USA	5705
Richard-Allan Scientific Histoplast Paraffin	Thermofisher, USA	8330

Shandon™ Harris Hematoxylin	Thermofisher, USA	6765002
Shandon™ Eosin Y	Thermofisher, USA	6766010
Lipofectamine™ 3000 Transfection Reagent	Thermofisher, USA	L3000001
CM-H2DCFDA	Thermofisher, USA	C6827
MitoTracker™ Green FM	Thermofisher, USA	M7514
MitoTracker™ Deep Red FM	Thermofisher, USA	M22426
ProLong™ Glass Antifade Mountant	Thermofisher, USA	P36980
SlowFade™ Gold Antifade Mountant with DAPI	Thermofisher, USA	S36938
Trypan Blue Stain (0.4%)	Thermofisher, USA	T10282
2×Es Taq MasterMix	CoWin Biosciences, China	CW0690
QuantiNova SYBR Green PCR Kit	Qiagen, Germany	208057
DNeasy Blood & Tissue Kit	Qiagen, Germany	69504
Insulin, Human Recombinant	Sigma-Aldrich, USA	91077C
Ammonium persulfate	Sigma-Aldrich, USA	A3678
Bovine serum albumin	Sigma-Aldrich, USA	05470

Bovine Serum Albumin (fatty acid-free, low endotoxin)	Sigma-Aldrich, USA	A8806
Proteinase K from Tritirachium album	Sigma-Aldrich, USA	P2308
D-(+)-Glucose	Sigma-Aldrich, USA	346351
Sodium chloride	Sigma-Aldrich, USA	S9888
Sodium bicarbonate	Sigma-Aldrich, USA	S5761
Immun-Blot PVDF Membrane	Bio-Rad, USA	1620177
GoScript™ Reverse Transcription Mix, Random primers	Promega Corporation, USA	A2801
Recombinant Mouse IFN-gamma Protein	R&D Systems, USA	485-MI
Medical X-ray film	Fuji, Japan	Super HR-U30
Protease Inhibitor Cocktail	MedChemExpress, USA	HY-K0010
Phosphatase Inhibitor Cocktail	Bimake, USA	B15002
2-Mercaptoethanol	Bio-Rad, USA	1610710
Clarity Western ECL Substrate	Bio-Rad, USA	1705061
Clarity Max Western ECL Substrate	Bio-Rad, USA	1705062
Ultrapure flagellin from S. Typhimurium	InvivoGen, USA	tlrl-epstfla

Muramyl dipeptide	InvivoGen, USA	tlrl-mdp
Monosodium Urate Crystals	InvivoGen, USA	tlrl-msu
Palmitic Acid	Cayman Chemical, USA	10006627

2.1.2 Biochemical assays

Assay	Provider	Catalog number
Pierce™ BCA Protein Assay Kit	Thermofisher, USA	23225
High Sensitive Mouse Insulin ELISA Kit	ImmunoDiagnostics Limited, Hong Kong	32270
Mouse Adiponectin ELISA Kit	ImmunoDiagnostics Limited, Hong Kong	32010
Aspartate Transaminase Kit	Stanbio, USA	2930-430
Alanine Transaminase Kit	Stanbio, USA	2930-500
Cholesterol Kit	Biosino, China	20162400910
Free fatty acid kit	Biosino, China	20162401089
Triglycerol Kit	Biosino, China	20162400911
HDL-C kit	Biosino, China	20152400950
LDL-C kit	Biosino, China	20162400518

2.1.3   Primer sequences

Species	Gene name	Primer sequences (5'-3')	
		Forward	Reverse
Mouse	GPR110	CCAAGAGAAGCCAAACCTCC	TTCGATAAGCCAGCAGGATG
	SCD1	CTGACCTGAAAGCCGAGAAG	AGAAGGTGCTAACGAACAGG
	GAPDH	ACTCCACTCACGGCAAATTC	TCTCCATGGTGGTGAAGACA
	Albumin	ACAGGACACCTGCTCTC	AGTCCTGAGTCCTTCATGTCTTT
	F4/80	CTTTGGCTQTGGGCCTTCCAGTC	GCAAGGAGGACAGAGTTTATCGTG
	CD11b	ATGGACGCTGATGGCAATACC	TCCCCATTCACGTCTCCCA
	ACOT1	ACTACGATGACCTCCCCAAG	CATAGCAAGGCCAAGTTCAC
	Cy4a12b	GTTCCTACAGATTTCTAGCTCCC	AGAGTCTGCCATGATTTCCG
	Cy4a31	CACTCATTCCTGCCCTTCTC	ACAATCACCTTCAGCTCACTC
	ACACA	AAGGCTATGTGAAGGATGTGG	CTGTCTGAAGAGGTTAGGGAAG
	PCSK9	TTTTATGACCTCTTCCCTGGC	ATTCGCTCCAGGTTCCATG
	MRPL53	TCAAGCTGGTTCGAGTTCAG	ACAGAGCAGTTGAGGTTGG

	HSPD1	AGTGTTCAGTCCATTG TCCC	TGACTGCCACAACCTG AAG
	PLTP	CCTGTGCTCTACCATG CTG	ATTCCATATCCAGGTT GCCG
	ABCA1	TGACATGGTACATCG AAGCC	GATTTCTGACACTCCC TTCTGG
	FGF21	ACGACCAAGACACTG AAGC	ACCCAGGATTTGAAT GACCC

2.1.4 Antibodies

Antibody name	Catalog number	Producer
Rabbit anti-GPR110	orb157302	Biorbyt
Rabbit anti-SCD1	ab236868,	Abcam
Mouse anti-GAPDH	40004-I-Ig	Proteintech
Rabbit anti-CD11b	ab133357	Abcam
Rabbit anti-albumin	ab207327	Abcam
Mouse anti-beta tubulin	66246-I-Ig	Proteintech
Mouse anti-beta actin	60008-I-Ig	Proteintech
Mouse anti-flag tag	66008-2-Ig	Proteintech

2.1.5   Buffers

Medium and buffer	Recipe
Complete growth DMEM	DMEM supplemented with 10% fetal bovine serum (FBS) and 1% penicillin and streptomycin (PS)
BMDM differentiation medium	Complete growth DMEM with 20% L929 conditioned medium
Phosphate buffered saline (PBS)	137 mM NaCl, 2.7 mM KCl, 4.3 mM Na_2HPO_4, 1.4 mM KH_2PO_4 (pH 7.4)
Radioimmunoprecipitation (RIPA) buffer	150 mM NaCl, 50 mM Tris HCl, 2 mM EDTA, 0.1%SDS, 1% NP-40 (pH 7.4)
Red blood cell (RBC) lysis buffer	155 mM NH_4Cl, 10 mM $KHCO_3$, 0.1 M EDTA
Sodium citrate buffer	0.1 mol/L sodium citrate, 0.1% Tween 20, pH 6.0
Tris-Acetate EDTA (TAE)	40 mM Tris-acetate, 2 mM EDTA, pH 8.0

SDS-PAGE running buffer	25 mM Tris, 192 mM glycine, 0.1% SDS (pH 8.3)
Transfer buffer	25 mM Tris, 192 mM glycine (pH 8.3)
Tris-buffered saline, 0.1%Tween 20 (TBST)	20 mM Tris, 150 mM NaCl, (pH 7.6)
5X SDS loading dye	250 mM Tris-Cl (pH 6.8), 0.05% Bromophenol blue, 50% Glycerol, 10% SDS, 5% 2-Mercaptoethanol

2.1.6   Diets

Diet	Provider	Catalog number
PicoLab® Rodent Diet 20	LabDiet	5053
Rodent Diet With 45 kcal%Fat	Research Diets	D14251

2.2   Methods

2.2.1 Animal studies

2.2.1.1   Animal maintenance

8-week-old male C57BL/6N mice were purchased from our Laboratory Animal Unit. Mice were housed in pathogen-free conditions at controlled temperature (23 ± 1 ℃) with a 12-hour light-dark cycle and access to food and water *ad libitum*. The 8-week-old male mice were divided into two groups and fed with either standard chow diet (STC, 18.3% protein, 10.2% fat, 71.5% carbohydrates, Research Diet Inc., New Brunswick, NJ, USA) or high-fat diet (HFD, 35% kcal carbohydrates, 20% kcal protein, Research Diets Inc., New Brunswick, NJ, USA) for 12 weeks.

For AAV2/8 transduction, in order to perform AAV2/8 transduction, 3×10^{11} copies of AAV2/8 vectors carrying either green fluorescent protein (GFP) or GPR110 were administered intravenously to 8-week-old male C57BL/6N mice with either STC or HFD diet. For antisense oligonucleotide (ASO) delivery, ASOs encoding GPR110 or negative control sequences were injected subcutaneously once a week at 5mg/kg to 8-week-old male C57BL/6N with either STC or HFD feeding. For inhibitor delivery, either SCD1 inhibitor (MK-8245) or vehicle were given to mice fed with HFD i.g. at the dose of 10mg/kg once a week.

2.2.1.2 Body composition analysis

Lean mass and fat mass of mice were quantitatively accessed by using the Minispec LF90 Body Composition Analyzer (Bruker, Massachusetts, USA).

2.2.1.3 Metabolic/behavioral phenotyping analysis

Analyses of the metabolic and behavioral phenotypes of m ice were monitored for simultaneous measurements, such as their total body energy expenditure, physical activity, indirect calorimetry, food intake, and water intake. Oxygen consumption (VO_2) and carbon dioxide production (VCO_2) by mice were measured continuously thus respiratory exchange ratio (RER) can be calculated by using the metabolic cage system (Promethion, Nevada, USA). Mice were housed individually in metabolic cages and acclimatized under controlled temperature (23 ± 1 °C) with free access to water and food for 24 hours before start measurement and the data collection. VO_2 and heat generation were recorded every 11 min for a course of 2 days. Energy expenditure was calculated by normalizing heat generation to lean mass.

2.2.1.4 Intraperitoneal glucose tolerance test (GTT)

Mice were fasted for 16 hours with free access to water before the experiment. Basal level of fasting blood glucose and fasting body weight were obtained before D-glucose solution i.p. injection (2g/kg BW). Glucose levels of mice were measured by collecting the blood samples from the tip of the tail at the time point of 0, 15, 30, 60, 90 and 120-minute after injection.

The glucose level in these samples were measured by the Accu-Chek®
glucometer (Roche Diagnostics, Indiana, USA).

2.2.1.5   Intraperitoneal insulin tolerance test (ITT)

Mice were fasted for 8 hours with free access to water before the experiment.
Basal level of fasting blood glucose and fasting body weight were obtained
before insulin i.p. injection (0.4IU/kg BW). Glucose levels of mice were
measured by collecting the blood samples from the tip of the tail at the time
point of 0, 15, 30, 60, 90 and 120-minute after injection. The glucose level
in these samples were measured by the Accu-Chek® glucometer (Roche
Diagnostics, Indiana, USA).

2.2.1.6   Intraperitoneal pyruvate tolerance test (PTT)

Mice were fasted for 16 hours with free access to water before the
experiment. Basal level of fasting blood glucose and fasting body weight
were obtained before i.p. injection of sodium pyruvate solution (1g/kg BW).
Glucose levels of mice were measured by collecting the blood samples from
the tip of the tail at the time point of 0, 15, 30, 60, 90 and 120-minute after
injection. The glucose level in these samples were measured by the Accu-
Chek® glucometer (Roche Diagnostics, Indiana, USA).

2.2.1.7 Lipid profile analysis

Serum levels of triglyceride (TG) and total cholesterol (CHO) were measured using commercial kit (Biosino bio-technology and science INC, China) according to the manufacturer's instructions. Serum levels of free fatty acid (FFA) were measured using commercial kit (Solarbio, China) according to the manufacturer's instructions.

2.2.1.8 Liver damage analysis

Serum aspartate aminotransferase (AST) and alanine aminotransferase (ALT) levels were measured using commercial kits (Stanbio, EKF diagnostics, USA) according to the manufacturer's instructions.

2.2.1.9 Insulin level

Following the manufacturer's instructions, commercial kits (Mercodia, Sweden) were used to assess the serum insulin levels of mice.

2.2.2 Cell culture and *ex vivo* studies

2.2.2.1 Isolation of hepatocyte and nonparenchymal cells (NPCs)

Primary hepatocytes and NPCs were isolated from mouse liver from 8-week-old male C57BL/6N mice as previously described (83). Briefly, mice were anesthetized and subjected to *in situ* liver perfusion. 10 ml 1 X PBS supplemented with 0.05% (w/v) Type I collagenase were perfused through

suprahepatic inferior vena cava at flow rate of 10 ml/min. The gallbladder was subsequently removed, and the liver was incubated in serum-free DMEM at 37℃. The liver was cut into small pieces and mesh in serum-free DMEM through a 70 µM cell strainer and pelleted by centrifugation at 50 ×g for 5min. The pellet was collected and washed by 1 X PBS twice for hepatocyte collection. Using two layers of gradient solutions, the supernatant after centrifugation was transported to the top of a new tube. The middle layer is 25% (v/v) Percoll in 1 X PBS and the bottom layer is 50% (v/v) Percoll in 1 X PBS. After centrifuging at 800×g for 20min at 4℃ without bake, the NPC cells were observed and collected in the middle of two Percoll solutions. The primary hepatocytes and NPCs were then used for RNA extraction and real-time PCR analysis.

2.2.2.2   Luciferase reporter assay

HEK293 cells were cultured in DMEM supplemented with 10% FBS, 100 U/ml penicillin and 100 μg/ml streptomycin at 37 ℃ and 5% CO_2. HEK293 cells were ceded in 6-well plates and were transfected with pGL3-SCD1 promoter and adenoviral vector expressing either GPR110 (ADV-GPR110) or GFP (ADV-GFP) by using the transfection reagent (#E4981, Promega, WI, USA), following the manufacturer's instruction. DHEA was purchased from APExBIO (C3270, APExBIO, TX, USA) and was added into cells at the concentration of 100 μM and incubated at 37 ℃ for 48h. Renilla luciferase reporter plasmid pRL-TK was applied as a transfection control for

the luciferase reporter test. The Dual-Luciferase Reporter Assay System (#E1960, Promega, WI, USA) was used for the luciferase assays.

2.2.3 Histological analysis

2.2.3.1 Tissue processing

Liver samples from different groups of mice were collected for histological analysis. The samples were first fixed with 10% Formalin for 24h, followed by dehydration processing with Excelisior ES tissue processor (Thermo Fisher Scientific, Waltham, USA). The procedures of the program are as follows:

Table 2.1. Protocol of tissue processing

Step	Reagents	Time (min)	Temperature (°C)
1	75% ethanol	45	RT
2	85% ethanol	45	RT
3	95% ethanol	30	RT
4	95% ethanol	45	RT
5	100% ethanol	45	RT
6	100% ethanol	45	RT
7	Xylene	45	RT
8	Xylene	45	RT
9	Paraffin wax	45	62

10	Paraffin wax	45	62

Paraffin-embedded tissues were sliced into 5 µm-thick section with a microtome and dried overnight at 37 ℃.

2.2.3.2   Hematoxylin and eosin (HE) staining

The sections were deparaffinized and rehydrated using distilled water, xylene, and ethanol with a lowering concentration. After that, the slices were subsequently stained with hematoxylin, blued in Scott's tap water, and eosin. The stained slides were then dehydrated in ethanol with increasing ethanol and xylene. The dehydrated slides were mounted using DPX mounting medium. The details of staining procedures were as follows. Each paraffinized tissue was evaluated three times, with an interval of 50 m between each level. The images were taken with a Nikon Eclipse Ci Binocular Ergonomic Microscope. Image J was used for the quantification of the slides.

Table 2.2. Procedure of H&E staining

Step	Reagents	Time (min)	Remarks
1	Xylene	15	Deparaffinisation
2	Xylene	15	
3	Xylene	15	
4	100% ethanol	5	Hydration
5	100% ethanol	5	
6	90% ethanol	2	
7	80% ethanol	2	
8	70% ethanol	2	
9	Distilled water	5	
10	Hematoxylin solution	2	-
11	Tap water	10	-
12	Distilled water	2	-
13	1% acid ethanol solution	5 sec	Differentiation
14	Tap water	10	-
15	Eosin solution	10	-
16	100% ethanol	10	Dehydration
17	100% ethanol	10	
18	100% ethanol	10	
19	Xylene	30	Clearance
20	Mounting medium (xylene-based)		-

2.2.3.3   Oil red O staining

Liver samples from each group of mice were collected and frozen in OCT medium. The frozen sections were sliced by CryoStar NX70 Cryostat (Thermo Fisher Scientific, Waltham, USA). The cryostat sections were 8-10 µm. The slides were stained by Oil Red O working solution with the details as followed:

Table 2.3. Procedure of Oil Red O staining

Step	Reagents	Time
1	60% isopropanol	2s
2	Oil Red O working solution	15min
3	60% isopropanol	2s
4	Haematoxylin solution	2
5	Mounting medium (water-based)	

2.2.4 Enzyme-linked immunosorbent assay (ELISA)

Serum levels of insulin were determined by using commercial ELISA kits (Mercodia, Uppsala, Sweden). Briefly, 25 µl samples or standards were added per well to a microplate. 100 µl of enzyme conjugate 1X solution was added to each well and the microplate was incubated on a plate shaker for 1 hour at room temperature. 350 µl of 1X wash buffer was used for washing

each well for 6 times. 200 µl substrate TMB was then added into each well and incubated for 15 min at room temperature. Subsequently. 50 µl of stop solution was added and the plate was placed on a shaker for 5 seconds for mixing. The absorbance was measured under 450nm within 30 minutes.

2.2.5 Generation and purification of recombinant adeno-associated virus (rAAV)

rAAV was generated as previously described (84). Briefly, 293T cell line (ATCC, Virginia, USA) was seeded in 150mm culture dish. DMEM supplemented with 10% FBS was used as culture medium. The 293T cell line were incubated in a humidified incubator at 37 ℃. When the confluency reached 80%, full medium with FBS was removed and replaced by the serum-free DMEM. The cells were transfected with 250 µl PEI solution along with 7 µg vector (pAAV-GPR110 or pAM2AA-GFP), 7 µg serotype plasmid (p5E18-VD2/8), and 7 µg helper plasmid (pXX6) for 6 h. Subsequently, the medium was replaced by DMEM supplemented with 10% FBS for the subsequent 72 h. The medium was collected and went through three freeze-thaw cycles. After that, the medium was centrifuged and the precipitation mixture was centrifuged at 1500 ×g for 30 min at 4 ℃. The pellet was washed in with DMEM supplemented with 10% FBS followed by centrifugation at 1500 ×g for 3 min at 4 ℃. The pellet was resuspended in 1X PBS. The titer (genome copies) of rAAV was determined by qPCR analysis according to the standard curve of corresponding plasmid.

2.2.6 Western blot Analysis

Both tissue and cell samples were added with RIPA buffer supplemented with protease inhibitors for protein extraction. The tissues were homogenized with Precellys 24 tissue homogenizer (Bertin Instruments). For cell lysis, after washing the cultured cell with PBS twice, RIPA was added to lyse cell and no homogenize is needed. Both the tissue homogenates and cell lysis were collected and transferred to a new tube, followed by centrifuged at 1500 rpm for 15 min at 4°C. The protein layer was collected and quantified using BCA Assay Kit (Solarbio, Beijing, China). The quantified protein was then denatured with loading dye and 2-mercaptoethanol at 95 °C on a heat block for 10 minutes. The denatured protein samples were stored at 4 °C fridges for further use. Each lane of a polyacrylamide gel had an equal amount of protein sample loaded onto it. The protein sample was separated using SDS-PAGE with a Mini TransBlot® Cell (Bio-Rad) at 100-120V constant voltage in running buffer and transferred onto a polyvinylidene difluoride (PVDF) membrane soaked in methanol at 10 V constant voltage on ice for 30 minutes. The membrane was blocked for an hour at room temperature in 10 ml of 10% non-fat skimmed milk in TBST, then incubated overnight at 4 °C with 5 ml of non-fat skimmed milk and the primary antibody. The membrane was then incubated with a secondary antibody diluted with 10% non-fat skimmed milk in TBST at a ratio of 1:2500 for an additional hour at room temperature. The membrane was then rinsed with 5 ml TBST for 5 minutes, three times. The

membrane was then processed for visualization after being rinsed with 5 ml TBST for 5 minutes three times. Using the ChemiDoc MP Imaging System, enhanced chemiluminescence agents were used to see the protein bands (BioRad, California, USA). The membrane was stripped by incubating it in stripping buffer for 30 minutes at 50 ℃. The membrane was then rinsed for 30 minutes with running tap water, then washed four times for 5 minutes with TBST. The membrane was then once again blocked for an additional hour with 10 ml of 10% non-fat skim milk before the above-mentioned primary antibody incubation.

2.2.7 Quantitative real time PCR analysis

2.2.7.1 Total RNA extraction

For RNA extraction from tissue samples, samples were first homogenized with with Precellys 24 tissue homogenizer (Bertin Instruments) in1 ml of TRIzol reagent (TaKaRa Bio Inc., Shiga, Japan) at 4℃. The homogenate was then centrifuged at 13000 rpm for 15 min at 4℃. The oily layer was removed to avoid interference with RNA extraction. 1 ml of TRIzol was added to each well of a 6-well plate in order to lyse the cells and extract the RNA from them. 250 l of chloroform was added to each sample after the previous stage and thoroughly mixed. Afterward, the mixture was centrifuged at 12000 rpm for an additional 15 minutes at 4 ℃. The top layer was removed and placed in a fresh tube. Subsequently, 200 µl of isopropanol was added to the new tube and incubated for 5 min at room temperature. The

samples were then centrifugated at 1200 rpm at 4 ℃ for 10 min to precipitated RNA. The RNA pellet was collected and washed with 1 ml 75% ethanol for 3 times by centrifuging at 7500 rpm, 5 min at 4 ℃. After that, the pellet was air-dry and the RNase-free water was used for resuspension. The concentration of RNA was quantified by NanoDrop™ 2000 Spectrophotometer (Thermo Scientific).

2.2.7.2 Reverse transcription

1 µg of total RNA was added for reverse transcribe into cDNA by using PrimeScript RT Reagent Kit (Takara Bio Inc, Shiga, Japan). The details of the transcription system were showed as follow:

Table 2.4. Set up for RT-PCR

Component	Volume
Reaction buffer	5 µl
dNTPs	1 µl
PrimeScript RTase	1 µg
Oligo dT primer	1 µl
Total RNA	1 µg
Nuclease-free water	Top up to 10 µl
Final volume	10 µl

2.2.7.3 Real-time quantitative PCR

cDNA was then amplified with TB green Premix Ex Taq^{TM} II (Til Rnase H Plus) (TakaRa Bio Inc., Shiga, Japan). The real-time PCR was conducted with the LightCycler 96 qPCR System (Roche, Basel, Switzerland). The relative quantity of the targeted RNA was calculated through normalization to the quantity of the corresponding GAPDH mRNA level. Detailed primer sequences were listed below.

2.2.8 Statistical analysis

All analyses were performed with GraphPad Prism 7 (GraphPad, California, USA). The results of three separate tests performed in triplicates were provided as means ± SEM. Sample sizes of animal studies were chosen on the basis of literature documentation of similar well-characterized experiments, and no statistical method was used to predetermine sample size. One-way analysis of variance (ANOVA), analysis of covariance (ANCOVA), or the Student's *t* test were used to establish the statistical significance. A statistically significant difference was defined in all statistical comparisons as one with a p value of 0.05 or lower.

Chapter 3 - GPR110 is a novel GPCR that ameliorates NAFLD in diet-induced obese mouse model

3.1   Introduction

Liver is a key organ that closely related to many physiological processes such as digestion, metabolism and immunity (86). Non-alcoholic fatty liver disease is the term used to refer to the excessive fat accumulation in the hepatocytes of the liver that is not driven on by alcohol (NAFLD). It is nowadays the most common pathological condition of liver. There are many different factors contributing the development of NAFLD like lipid metabolism disorders, over-nutrition and inflammation (87). Although NAFLD does not has any symptoms at early stage, it will lead to non-alcoholic steatohepatitis (NASH) with fibrosis, cirrhosis or even hepatocellular carcinoma (88). On the other hand, NAFLD accounts for approximately 85% of chronic non-communicable diseases (NCDs) such as type 2 diabetes mellitus (T2DM), cardiovascular disease (CVD) and chronic kidney disease (CKD) (89, 90). However, the current therapeutic strategy for NAFLD is by increasing physical exercise activity as well as reducing the hypercaloric diet. No medication is available to reverse the condition that the excessive fat storage in liver. Therefore, it is important to unravel the mechanism of NAFLD, in order to accelerate the development, implementation and explore new targets for the development of diagnostic test and cost-effective therapies (91).

GPCRs are reported to be the largest and most diverse family of membrane receptors that play crucial roles in regulating various cellular and

physiological processes (92). GPCRs are the main targets for authorized medicines on the market right today. There are a few GPCRs have been shown to play key roles in NAFLD as it is shown that modulating the activities of these receptors may ameliorate liver-related metabolic syndrome, which is proposed to be the potential treatment of NAFLD (93, 94). However, since these genes are nor exclusively expressed in hepatocytes, the potential side effects on other organs should be considered when using them as the treatment for NAFLD. To solve this problem, we screened for liver predominant GPCRs and explored the potential roles in the treatment of obese-induced NAFLD.

A class B orphan receptor called GPR110 is primarily expressed in the liver (77, 95). It is found that human GPR110 (hGPR110) has a highly conserved amino acid sequences of G protein coupled receptor transmembrane domains by phylogenetic analysis in 2002 (62). Mouse ortholog of hGPR110 was then identified by the same group in 2004 (77). Moreover, various splice variants were detected in deep sequencing experiments (75, 78). The majority of investigations on GPR110 to date have emphasized its function in cancer. GPR110 is necessary to increase cancer cell survival, proliferation, and migration and has been discovered to be overexpressed in a number of malignancies, including lung, prostate, and glioma. For these reasons, it is suggested that GPR110 may be a potential target for the anti-cancer drug target. However, it is illustrated that GPR110 is predominantly expressed in adult livers and the physiological function of hepatic GPR110 remains

unexplored. In this chapter, we first revealed the role of GPR110 in whole-body energy metabolism. Diet-induced obese (DIO) mouse model was used to explore the role of GPR110 in the pathogenesis of obese-related NAFLD. The metabolic phenotypes of mice were extensively investigated. GPR110 is a class B orphan receptor that is found mainly expressed in liver (77, 95). It is found that human GPR110 (hGPR110) has a highly conserved amino acid sequences of G protein coupled receptor transmembrane domains by phylogenetic analysis in 2002 (62). Mouse ortholog of hGPR110 was then identified by the same group in 2004 (77). Moreover, various splice variants were detected in deep sequencing experiments (75, 78). Currently, most GPR110 related studies focused on its role in cancer. In general, overexpression level of GPR110 was found in various cancers (lung, prostate, and glioma etc.) and it is required to promote cancer cell survival, proliferation, and migration. For these reasons, it is suggested that GPR110 may be a potential target for the anti-cancer drug target. However, it is illustrated that GPR110 is predominantly expressed in adult livers and the physiological function of hepatic GPR110 remains unexplored.

In this chapter, we first revealed the role of GPR110 in whole-body energy metabolism. Diet-induced obese (DIO) mouse model was used to explore the role of GPR110 in the pathogenesis of obese-related NAFLD. The metabolic phenotypes of mice were extensively investigated.

3.2   Results

3.2.1 Liver is the main organ expresses GPR110

According to previous report, GPR110 expression is mainly expressed in liver, as well as plays an important role in the pathogenesis of hepatic fibrosis (96). To confirm the expression pattern of this gene, various tissues including liver, kidney, brain and lung from 8-week-old C57BL/6J mice fed with STC diet. qPCR was conducted for mRNA level measurement and western blot was used for measuring the protein level, respectively. Consistently, GPR110 is mainly expressed in the liver of adult mice (Fig. 3.1A-B). After that, hepatocytes and Kupffer cells were isolated by cell fractionation to identify the GPR110 expressing cells in the liver. Non-parenchymal cells (NPC) and hepatocytes were identified using the markers CD11b and albumin, respectively. It is demonstrated that GPR110 mRNA is mainly expressed in hepatocytes (Fig. 3.1C). This finding was in consistent with protein levels by western blot analysis (Fig. 3.1D).
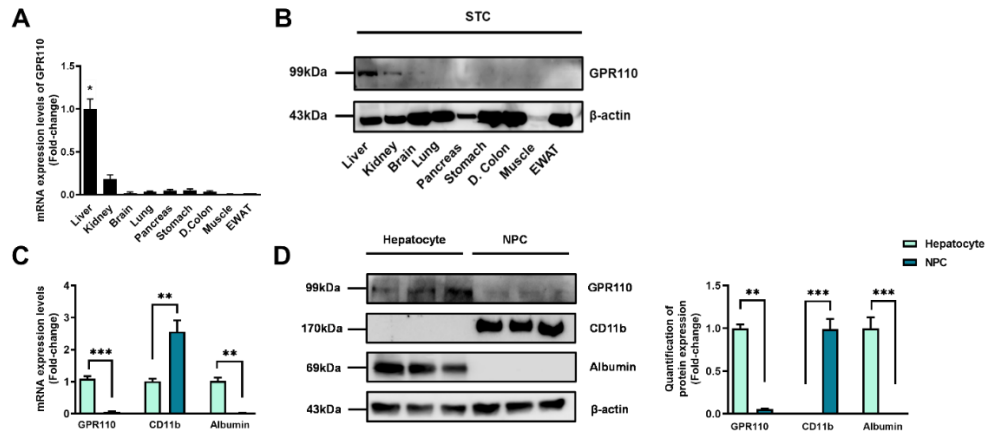
Figure 3.1. GPR110 is mainly expressed in the liver. (A) mRNA expression levels of GPR110 in different organs as determined by qPCR analysis. (B) Representative immunoblotting analyses of GPR110 expression in different tissues of C57BL/J mice after STC for 8 weeks. (C) GPR110, CD11b and albumin mRNA expression levels in hepatocytes determined by qPCR. (D) Representative immunoblotting analyses of GPR110, CD11b and albumin in fractions of hepatocytes or NPC isolated from the livers of mice fed with STC; each lane is a sample from individual mice. Data represent as mean ± SEM; n = 4-5 per group; repeated with three independent experiments; P value analyzed by two-tailed Student's *t* test. *P < 0.05, **P < 0.01, ***P < 0.001.

3.2.2 Hepatic GPR110 expression is tightly regulated by nutrient availability

Interestingly, after HFD treatment for 8 weeks, we found that the expression level of hepatic GPR110 was decreased to almost undetectable level as measured by qPCR (Fig. 3.2A). FGF21 and F4/80 (also named as ADGRE1) were used as reference gene which were significantly increased in the liver in mice fed with HFD (97, 98). Similarly, western blot result also indicated that the declined expression of GPR110 can be also detected in protein level in the liver of HFD-fed mice (Fig. 3.2B upper panel) while there was no difference detected in renal GPR110 expression (Fig. 3.2B lower panel). Therefore, the hepatic GPR110 expression level is tightly regulated by nutritional statuses.
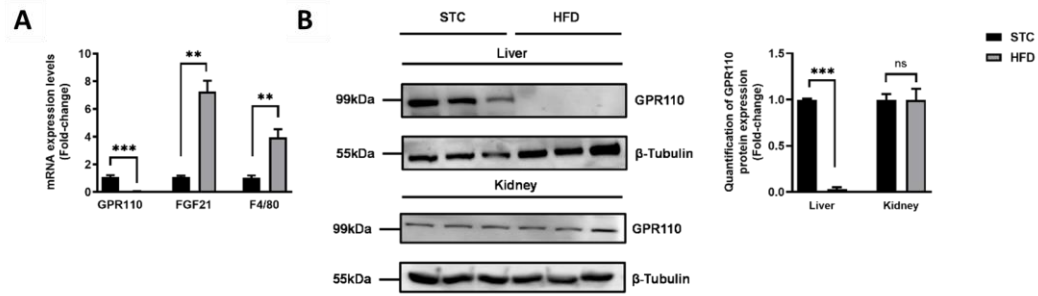
Figure 3.2. Hepatic GPR110 expression is tightly regulated by nutrient availability. (A) mRNA expression levels of GPR110, FGF21 and F4/80 (served as a HFD marker) in the livers of mice fed with either STC or HFD for 8 weeks as determined by qPCR. (B) Representative immunoblotting analyses of GPR110 in mice fed with either STC or HFD for 8 weeks. Each lane is a sample from individual mice. Data represent as mean ± SEM; n = 4-5 per group; repeated with three independent experiments; P value analyzed by two-tailed Student's *t* test. *P < 0.05, **P < 0.01, ***P < 0.001.

3.2.3 rAAV/ApoE-mediated gene expression system successfully increases the expression of GPR110 in hepatocytes

Based on the notable difference in hepatic GPR110 expression level before and after HFD treatment, we hypothesized that downregulation of GPR110 in HFD-fed mice may be implicated in the pathogenesis of obesity, such as fatty liver. GPR110 was overexpressed in the hepatocytes of DIO mice using a liver-directed rAAV/ApoE-mediated gene expression system to assess the effects of GPR110 on metabolism (Fig. 3.3A). By using qPCR and western blot analysis, the overexpression of GPR110 in the mice's livers was confirmed (Fig. 3.3B-C). Liver-directed rAAV/ApoE-mediated gene expression did not have an impact on the level of renal GPR110 expression (Fig. 3.3C). This result is consistent with the mice fed with HFD (Fig. 3.3 D-E). In addition, according to the cell fractionation, we noticed that the rAAV-mediated GPR110 overexpression was solely in hepatocytes, rather than in NPC (Fig. 3.3F).
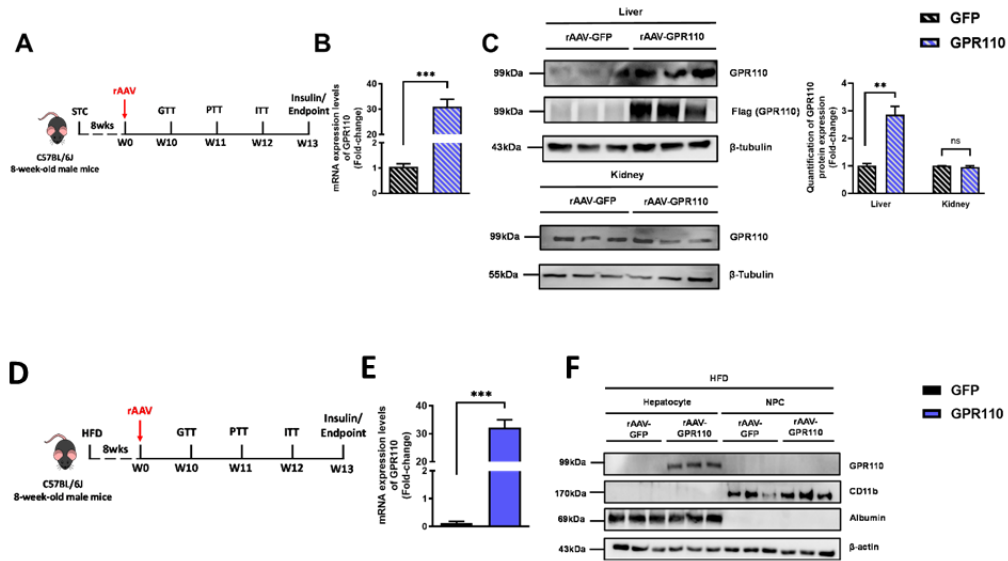
Figure 3.3. rAAV/ApoE-GPR110 increases the expression level of GPR110 in hepatocytes. (A) Schematic illustration of viral treatments. (B) Hepatic mRNA expression levels of GPR110 from rAAV-GPR110 STC-fed mouse livers. (C) Immunoblotting analysis of hepatic protein expression levels of GPR110 from rAAV-GPR110 mice. (D) Schematic illustration of viral treatments. (E) Hepatic GPR110 mRNA expression levels in hepatocytes or NPC from HFD-fed mouse livers. (F) Immunoblotting analyses of GPR110, CD11b and albumin from hepatocytes or NPC. Data represent as mean ± SEM; n = 8 mice per group; repeated with three independent experiments; P value analyzed by two-tailed Student's *t* test. *P < 0.05, **P < 0.01, ***P < 0.001.

3.2.4 Overexpression of GPR110 in hepatocytes only slightly accelerates metabolic dysregulation in STC mice

After injecting the rAAV-GPR110 in STC mice, the metabolic phenotypes were measured. However, it is found that overexpressing GPR110 in the liver of STC-fed mice will not affect body weight (Fig. 3.4A), fasting glucose level (Fig. 3.4B), fasting insulin level (Fig. 3.4C) and homeostatic model assessment for insulin resistance (HOMA-IR) (Fig. 3.4D). Only a slight increase at the time points of 30 and 60 min of glucose excursion curve in response to GTT (Fig 3.4E). Regarding the hepatic glucose production ability, the higher levels were only detected at the time point of 90 and 120 min in PTT (Fig. 3.4F). ITT revealed no differences in insulin sensitivity between rAAV-GFP and rAAV-GPR110 animals that were fed STC (Fig. 3.4G).

3.2.5 GPR110 overexpression only impacts triglyceride metabolism rather than other lipids in STC mice

Apart from the glucose related phenotypes, we also measured the lipid profile of rAAV-GPR110 mice. It was discovered that the serum CHO level in the GPR110 overexpression group was trending rising (p=0.06) (Fig. 3.5A). In comparison to the GFP group, the GPR110 overexpression group had a significantly higher level of serum TG (Fig. 3.5B), while no difference detected regarding the serum FFA content (Fig. 3.5C).
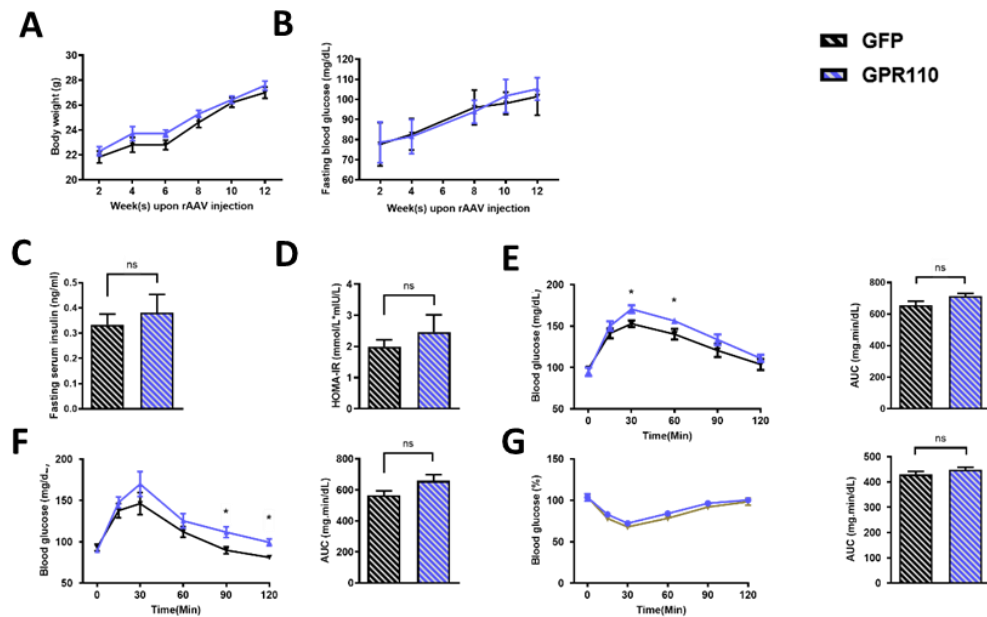
Figure 3.4. Overexpression of GPR110 in hepatocytes only slightly accelerates metabolic dysregulation in STC mice. (A) The change of body weight and (B) fasting blood glucose were measured. (C) Fasting blood insulin level and (D) HOMA-IR values were measured and calculated at the end the experiment. (E) GTT (1g/kg BW, left) and AUC (right) were measured. (F) PTT (1g/kg BW, left) and AUC (right) were conducted. (G) ITT (0.5 U/kg BW, left) and AUC (right) were conducted. Data represent as mean ± SEM; n = 8 mice per group; repeated with three independent experiments; P value analyzed by two-tailed Student's *t* test. *P < 0.05, **P < 0.01, ***P < 0.001.
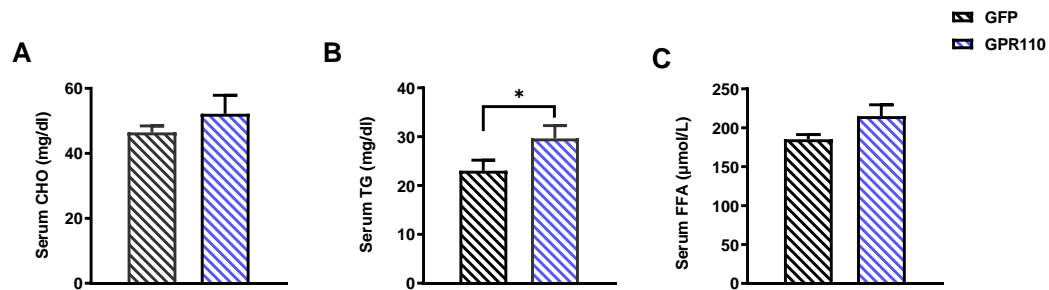
Figure 3.5. Mice with hepatic GPR110 overexpression had a higher serum triglyceride level. (A) Serum CHO, (B) serum TGs and (C) serum FFA levels. Data represent as mean ± SEM; n = 8 per group; repeated with three independent experiments; P value analyzed by two-tailed Student's t test. *$P < 0.05$, **$P < 0.01$, ***$P < 0.001$.

3.2.6 Overexpression of GPR110 in hepatocytes accelerates metabolic dysregulation caused by HFD

Interestingly, rAAV-GPR110 mice developed greater body weight and body fat mass under HFD treatment than their rAAV-GFP littermates (Fig. 3.6A). Besides, a higher percentage of fat mass (Fig. 3.6B) and a lower proportion of lean mass (Fig. 3.6C) were noticed in the GPR110 overexpression group. Moreover, the fasting glucose level (Fig. 3.6D), fasting insulin level (Fig. 3.6E) and HOMA-IR (Fig. 3.6F) were all higher in the HFD-fed rAAV-GPR110 mice. Increased glucose intolerance was detected in rAAV-GPR110 mice fed with HFD (Fig. 3.6G). Hepatic glucose production was dramatically boosted in PTT by overexpressing GPR110 in the livers (Fig. 3.6H). ITT demonstrated that when compared to their control HFD-fed rAAV-GFP littermates, glucose levels in HFD-fed rAAV-GPR110 mice remained unresponsive at 30 to 60 minutes following insulin injection (Fig. 3.6I). In conclusion, we found that overexpressing GPR110 in the livers of STC-fed mice led to a modest impairment in glucose homeostasis; however, a more severe impairment was found when HFD was imposed on the rAAV-GPR110 mice.
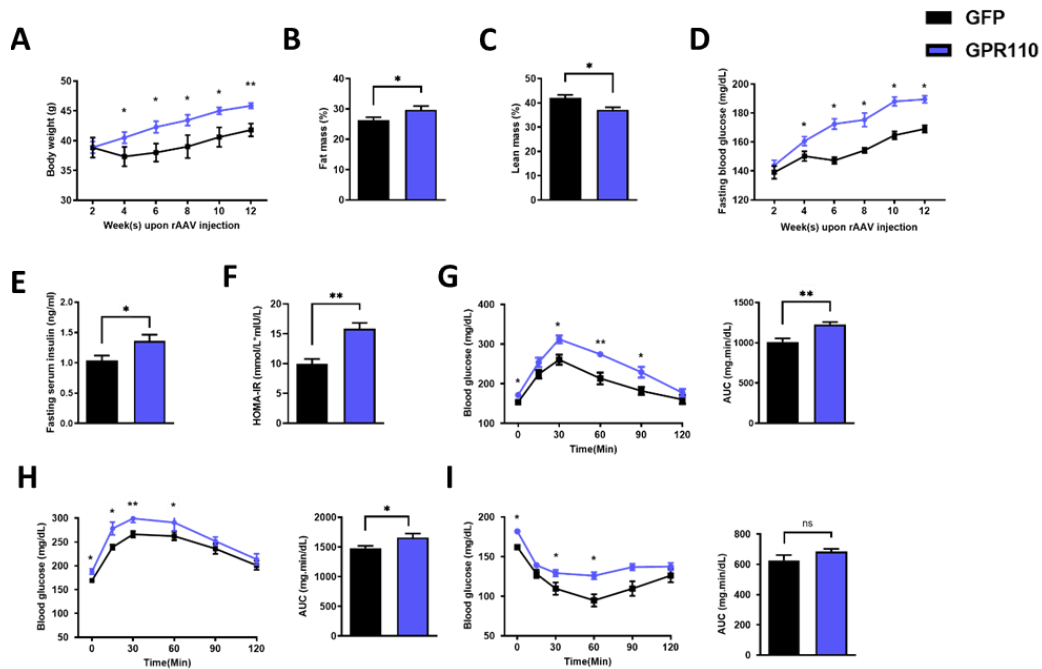
Figure 3.6. Overexpression of GPR110 in hepatocytes exaggerates metabolic dysregulation under HFD. (A) Body weight, (B) fat mass and (C) lean mass were assessed in different groups. (D) Fasting blood glucose level were measured biweekly. (E) The fasting serum insulin level and (F) HOMA-IR index were measured and calculated at the end of the experiment. (G) GTT (1g/kg BW, left) and AUC (right) of serum glucose. (H) PTT (1g/kg BW, left) and AUC (right) of serum glucose. (I) ITT (0.5 U/kg BW, left) and AUC (right) of serum glucose. Data represent as mean ± SEM; n = 8 mice per group; repeated with three independent experiments; P value analyzed by two-tailed Student's *t* test. *P < 0.05, **P < 0.01, ***P < 0.001.

3.2.7 GPR110 overexpression exacerbates the lipid disorder in HFD mice

In addition, we also assessed the content of circulating lipids in those rAAV-GPR110 mice to explore if there have any changes in the lipid metabolism. Surprisingly, comparing to the STC mice, the gap of serum CHO was increased and can be observed in those GPR110 overexpression mice with HFD-fed (Fig. 3.7A). The significantly higher content of circulating TG can still be detected in the overexpression mice after HFD treatment (Fig. 3.7B). However, there remained no difference regarding the serum FFA level between these two groups (Fig. 3.7C). Collectively, hepatic overexpression of GPR110 accelerated the severity of obesity as well as the progress the glucose intolerance, especially after HFD treatment. The GPR110 overexpression mice also shown to have a worse lipid profile in DIO mice.
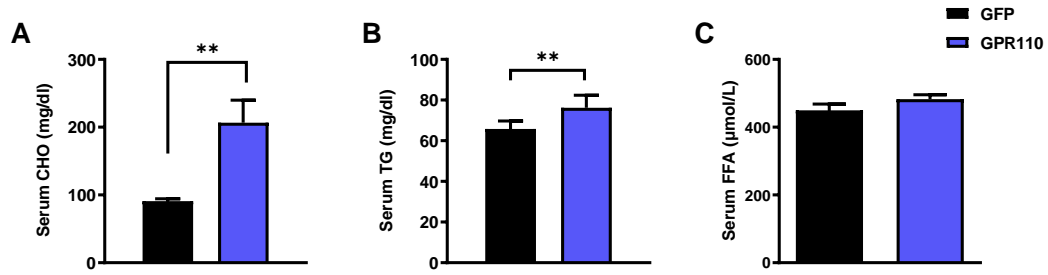
Figure 3.7. GPR110 overexpression accelerates the disorder of lipid metabolism. (A) Serum CHO, (B) serum TGs and (C) serum FFA levels. Data represent as mean ± SEM; n = 8 per group; repeated with three independent experiments; P value analyzed by two-tailed Student's *t* test. *P < 0.05, **P < 0.01, ***P < 0.001.

3.2.8 Hepatic knockdown of GPR110 does not affect the metabolic phenotypes in STC mice

Based on the data above, we found that the overexpression of hepatic GPR110 may lead to a worse metabolic disorder in HFD mice. Therefore, to confirm that these findings were due to the overexpression of GPR110, two sequences of N-acetylgalactaosamine (GalNAc) conjugated antisense oligonucleotides (ASO-GPR110s), targeting to different regions of GPR110 mRNAs, were used to knockdown the hepatic expression of GPR110 in mice.

We used ASO-GPR110s to knockdown the hepatic expression in STC mice to explore if there has any difference between the control group (Fig. 3.8A). Since ASOs will degraded in the body within 7 days, we kept injecting the sequences into mice every five days to make sure the hepatic GPR110 expression is knockdown. We first confirm the knockdown effect by qPCR analysis. It is shown that only hepatic GPR110 had a lower expression in the knockdown while no difference detected in renal GPR110 expression (Fig. 3.8B), implying that using ASO-GPR110 can efficiently knockdown the expression level in the liver. Western blot analysis also shown the similar results at protein level, where hepatic GPR110 protein level in both ASO-GPR110s were significantly lower than the negative control -scrambled ASO (ASO-NC) group (Fig. 3.8C).

However, based on our observations, chronic knockdown of hepatic GP110 by ASO-GPR110 treatment for 4 weeks does not affect the body weight (Fig.

3.9A) and fasting blood glucose (Fig. 3.9B), but slightly lowered insulin

level (Fig. 3.9C) and HOMA-IR (Fig. 3.9D) when compared to their ASO-

NC littermates. Moreover, regarding to the glucose metabolism, no

differences detected in GTT (Fig. 3.9E), PTT (Fig. 3.9F) and ITT (Fig. 3.9G)

between ASO-GPR110s and ASO-NC groups under STC feeding conditions.

3.2.9   Knockdown of hepatic GPR110 does not affect the circulating lipid abundance in STC mice

Except for the glucose related phenotypes, we also measured the lipid profile

of ASO-GPR110s mice. It was illustrated that although there has a slightly

decrease in the level of serum CHO, no statistical significance can be found

among these three groups (Fig. 3.10A). Similar results can also be found in

serum TG (Fig. 3.10B) and serum FFA (Fig. 3.10C).
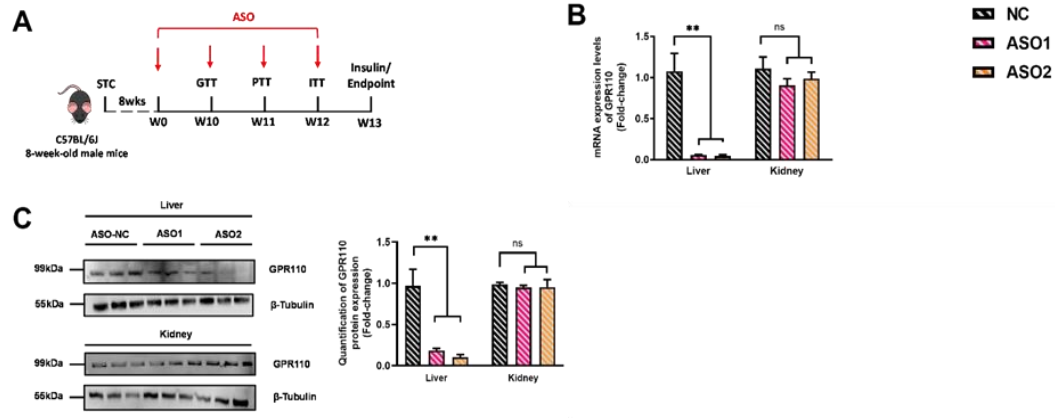
Figure 3.8. ASO-GPR110 can knockdown the hepatic GPR110 expression level. (A) Schematic illustration of viral treatments. (B) mRNA expression levels of GPR110 in liver and kidney as determined by qPCR analysis. (C) Immunoblotting analysis of hepatic protein expression levels of GPR110 from livers from STC-fed mice with GPR110 knockdown. Each lane is a sample from individual mice. Data represent as mean ± SEM; n = 8 mice per group; repeated with three independent experiments; P value analyzed by two-tailed Student's *t* test. *P < 0.05, **P < 0.01, ***P < 0.001.
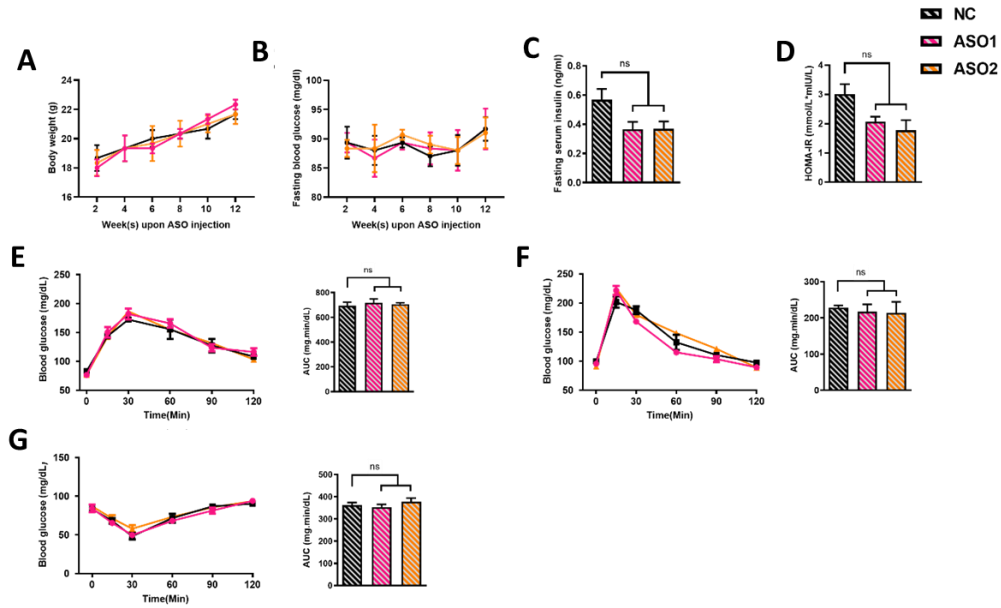
Figure 3.9. Hepatic knockdown of GPR110 does not affect the metabolic phenotypes in STC mice. (A) Change of body weight and (B) fasting blood glucose at different weeks were measured. (C) Fasting blood insulin level and (D) HOMA-IR values were measured and calculated at the end the experiment. (E) GTT (1g/kg BW, left) and AUC (right) of serum glucose. (F) PTT (1g/kg BW, left) and AUC (right) of serum glucose. (G) ITT (0.5 U/kg BW, left) and AUC (right) of serum glucose. Data represent as mean ± SEM; n = 8 mice per group; repeated with three independent experiments; P value analyzed by two-tailed Student's *t* test. *P < 0.05, **P < 0.01, ***P < 0.001.
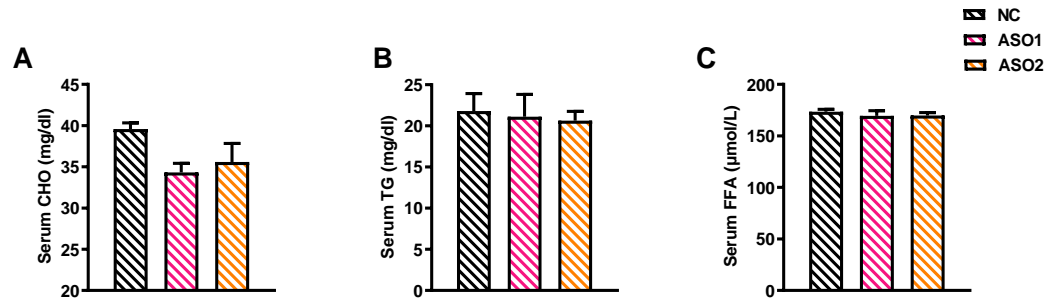
Figure 3.10. Hepatic knockdown of GPR110 does not modulate the circulating lipid levels in STC mice. (A) Serum CHO, (B) serum TGs and (C) serum FFA levels. Data represent as mean ± SEM; n = 8 per group; repeated with three independent experiments; P value analyzed by two-tailed Student's *t* test. *$P < 0.05$, **$P < 0.01$, ***$P < 0.001$.

3.2.10   Suppressing GPR110 improves glucose homeostasis in HFD-fed rAAV-GPR110 mice

Since the hepatic GPR110 will decrease to nearly undetectable after HFD treatment, we used ASO-GPR110s to knockdown the expression level in mice which were already had the rAAV-GPR110 overexpression in liver to further confirm the physiological role of GPR110 (Fig. 3.11A). First, we checked both the overexpression and knockdown effect in those HFD mice. Both qPCR and western blot results demonstrated that the mRNA and protein level were decreased after receiving the ASO-GPR110s (Fig. 3.11B-C).

In contrast to the STC-fed mice, chronic treatment of ASO-GPR110s will lead to a significantly decrease in body weight (Fig. 3.12A) and fat mass ratio (Fig. 3.12B-C). A lower fasting blood glucose (Fig. 3.12D) and a higher fasting insulin level (Fig. 3.12E) were also detected after the chronic ASO treatment in GPR110 overexpression mice. A lower HOMA-IR (Fig. 3.12F) was found in those ASO-GPR110 mice. Furthermore, when comparing to ASO-NC group, treatments of ASO-GPR110s improved glucose tolerance, pyruvate tolerance as well as insulin sensitivity in HFD-fed rAAV-GPT110 mice as illustrated by GTT (Fig. 3.12G), PTT (Fig. 3.12H) and ITT (Fig. 3.12I). These findings were consistent with previous data, implying that the deletion of hepatic GPR110 by ASOs improved glucose homeostasis in HFD-fed mice.
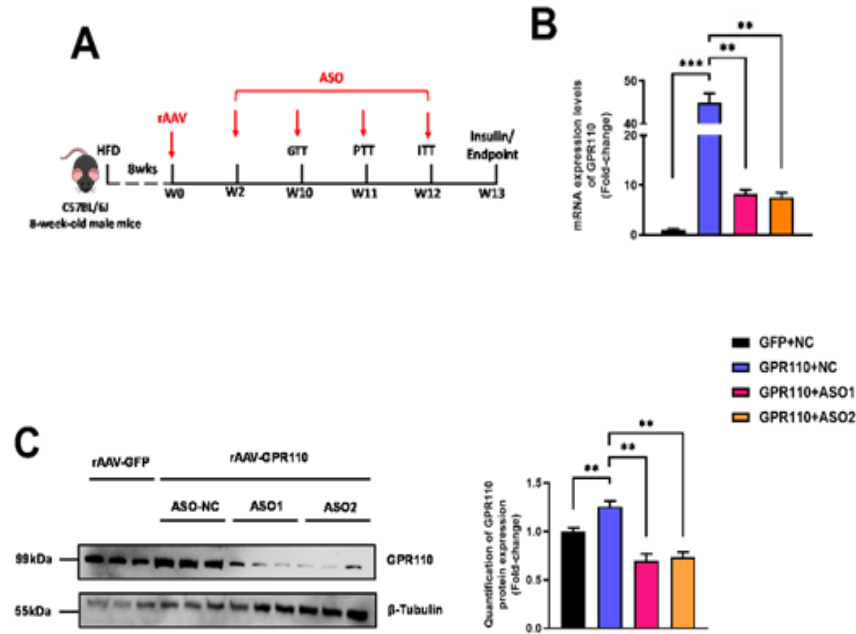
Figure 3.11. ASOs knockdown the hepatic GPR110 expression in GPR110-overexpressing HFD-fed mice. (A) Schematic illustration of viral treatments. (B) Hepatic mRNA expression levels of GPR110 from different groups of mice received either GFP-NC, GPR110-NC, GPR110-ASO1 or GPR110-ASO2, mice were fed with HFD, respectively, as determined by qPCR analysis. (C) Immunoblotting analysis of hepatic protein expression levels of GPR110 from HFD-fed mouse liver with GPR110 overexpression and knockdown. Each lane is a sample from individual mice. Data represent as mean $\pm$ SEM; n = 8 mice per group; repeated with three independent experiments; P value analyzed by two-tailed Student's *t* test. *P $<$ 0.05, **P $<$ 0.01, ***P $<$ 0.001.
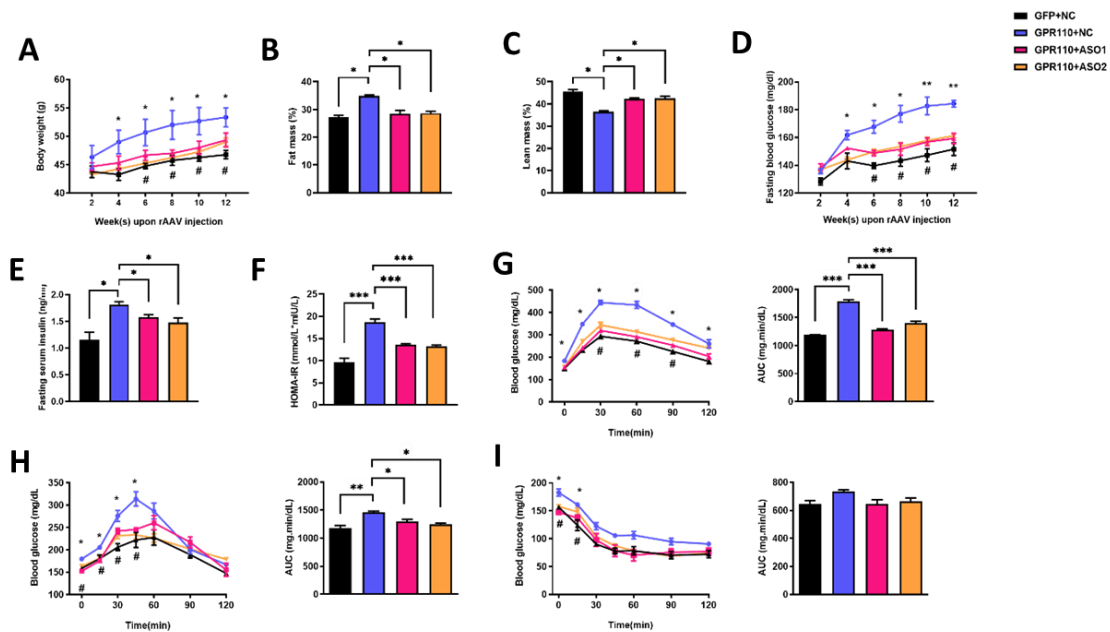
Figure 3.12 Suppressing GPR110 improves glucose homeostasis in rAAV-GPR110 mice fed with HFD. (A) Body weight, (B) fat mass, (C) lean mass were measured at the end of the experiment. (D) The fasting blood glucose level. (E) Fasting serum insulin level and (F) HOMA-IR index were measured and calculated at the end of the experiment. (G) GTT (1 g/kg BW), (H) PTT (1 g/kg BW, left) and (I) ITT (0.5 U/kg BW, left) and AUC (right) of serum glucose. Data represent as mean ± SEM; n = 8 mice per group; repeated with three independent experiments; P value analyzed by two-tailed Student's *t* test. *P < 0.05, **P < 0.01, ***P < 0.001.

3.2.11   Treatment of ASO-GPR110s improves serum lipid profiles and attenuates liver damage in HFD-fed rAAV-GPR110 mice

On the other hand, we also checked the circulating lipid profiles of these mice to explore whether there will have any differences after injecting ASO-GPR110s. It is found that HFD-fed rAAV-GPR110 mice had higher circulating CHO and TG levels than their rAAV-GFP littermates, but the levels were decreased after receiving chronic ASO treatment (Fig. 3.13A-B). No difference was observed in the circulating FFA levels among these groups (Fig. 3.13C). In addition, a higher HDL level can by detected in HFD mice with hepatic GPR110 overexpression, but the content was decreased after chronic ASO treatment. In contrary, regarding the LDL level, GPR110 overexpression leaded to a significantly increase but neither ASO-GPR110 can reverse it (Fig. 3.13D). Notably, when measuring the level of liver enzymes aspartate transaminase (AST) and alanine aminotransaminase (ALT), which were generally used as markers of liver damage and hepatoxicity, we found that in rAAV-GPR110 mice, the levels of these enzymes were remarkably increased. After receiving the chronic ASO-GPR110 treatment, the levels were decreased to their control littermates (Fig. 3.13E).
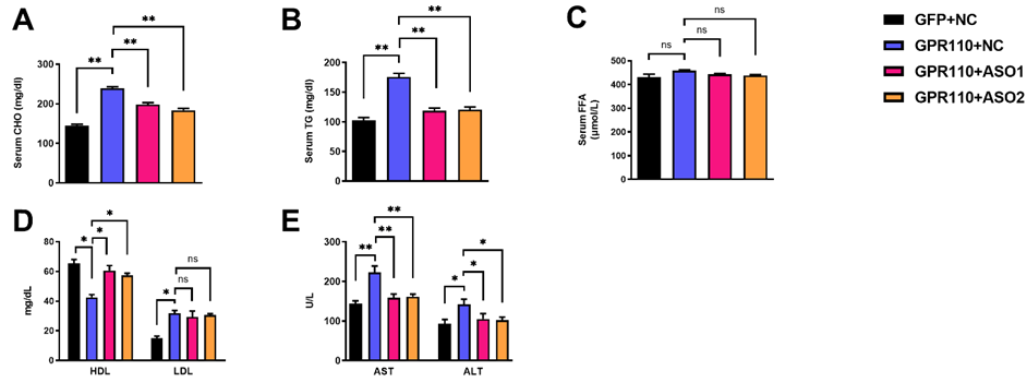
Figure 3.13 Treatment with ASO-GPR110s leads to an improved lipid profiles and alleviated liver damage in HFD-fed mice with rAAV-GPR110 overexpression. (A) Serum CHO, (B) serum TGs and (C) serum FFA levels measured at week 13. (D) Serum HDL and LDL. (E) The levels of serum AST, ALT. Data represent as mean ± SEM; n = 8 mice per group; repeated with three independent experiments; P value analyzed by two-tailed Student's *t* test. *P < 0.05, **P < 0.01, ***P < 0.001.

3.2.12 Knockdown of hepatic GPR110 in overexpressing mice alleviates hepatic steatosis in HFD mice

Since we found that the change of body weight among these groups were very dramatic, we measured the liver wight / body weight ratio to see whether the liver weight also changed under different conditions. It is shown that the HFD-fed rAAV-GPR110 mice were much heavier (Fig. 3.14A) and paler (Fig. 3.14B, upper panel) than that from their rAAV-GFP littermates and ASO-GPR110s. According to haematoxylin and eosin (H&E) staining (Fig. 3.14C, middle panels) and Oil Red O staining (Fig. 3.14D; lower panels), HFD-induced lipid deposits within hepatocytes were significantly more abundant in the livers of HFD-fed rAAV-GPR110 mice than the rAAV-GFP littermates.

3.2.13 GPR110 knockdown improves the hepatic lipid profile in HFD-fed GPR110 overexpression mice

The hepatic lipid profiles of rAAV-GRP110 animals, including CHO (Fig. 3.15A), TG (Fig. 3.15B), and FFA (Fig. 3.15C), may be improved by treatment with ASO-GPR110s for 8 weeks, similar to the circulating lipid profiles indicated above. In conclusion, overexpressing hepatic GPR110 in mice is enough to disrupt lipid metabolism, which in turn retards the development of NAFLD.
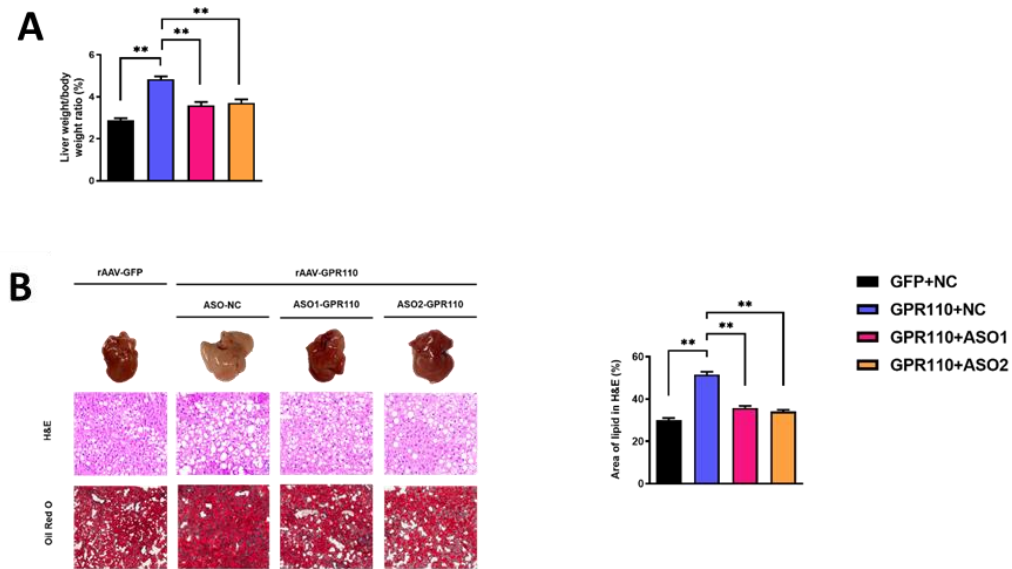
Figure 3.14 Overexpression of hepatic GPR110 results in a heavier and paler liver in HFD mice while down-regulation of hepatic GPR110 protects against the lipid accumulation. (A) The ratio of the liver weight against body weight were calculated after sacrificing the mice from four different groups. (B) Representative gross pictures of liver tissues (upper panels), representative images of H&E (middle panels) and Oil Red O (lower panels) staining of liver sections (200μm). The percentage of lipid area according to H&E staining (right panel). Data represent as mean ± SEM; n = 8 mice per group; repeated with three independent experiments; P value analyzed by two-tailed Student's *t* test. *P < 0.05, **P < 0.01, ***P < 0.001.
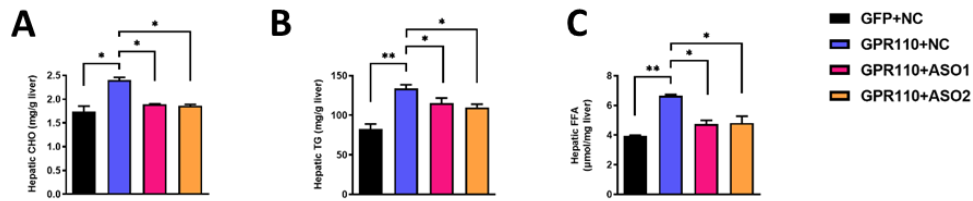
Figure 3.15. Up-regulation of hepatic GPR110 exaggerates liver steatosis mice fed with HFD while down-regulation of hepatic GPR110 protects mice from diet-induced liver lipid accumulation. (A) Hepatic CHO, (B) hepatic TG and (C) hepatic FFA were normalized by the weight of liver samples used for lipid extraction. Data represent as mean ± SEM; n = 8 mice per group; repeated with three independent experiments; P value analyzed by two-tailed Student's *t* test. *$P < 0.05$, **$P < 0.01$, ***$P < 0.001$.

3.3   Summary

In this chapter, we first confirmed that both GPR110 mRNA and protein is mainly expressed in liver. Based on the cell fractionation, we identified that this gene was expressed in hepatocytes but not Kupffer cells in the liver. Besides, our finding illustrated that the expression level of hepatic GPR110 was closely regulated by the nutrient availability and the content will dramatically decreased after HFD treatment. Furthermore, we used rAAV-GPR110 to build the hepatic GPR110 overexpression mice models and revealed that when mice were fed with STC, there was no obvious changes can be detected in the overexpression group when compared to the rAAV-GFP littermates. However, when mice were treated with HFD, hepatic GPR110 overexpression will lead to a worse ability of glucose metabolism as well as the lipid profile. To further confirm the physiological role of hepatic GPR110, we then used ASO-GPR110 to knockdown its hepatic expression level. Similar to the overexpression group, no differences were detected in mice treated with STC. But after receiving the chronic ASO-GPR110 treatment for four weeks, the glucose intolerance and lipid disorders were alleviated in HFD-fed rAAV-GPR110 mice. Moreover, apart from the circulating lipids, the HDL, AST, ALT and hepatic lipid profiles were also shown to be improved after chronic ASO treatment to knockdown the hepatic expression of GPR110.

Chapter 4 - The metabolic disorder of rAAV-GRP110 mice is correlated to the upregulated expression of SCD1

4.1 Introduction

NAFLD is due to the excessive fat accumulation in the liver, which may consequently result in a series of hepatic abnormalities such as hepatic fibrosis and chronic inflammation. Notably, recent research revealed that there are many different types of factors will be contributing to the pathogenesis of NAFLD (99, 100). It is reported that the two major causes result in the occurrences of NAFLD is lipid accumulation in hepatocytes and inflammation injury (101). Therefore, it is definitely associated with a reprogramming of hepatic metabolism, causing from disorders of major molecular mechanisms and gene expression which is involved in hepatic lipid metabolism (102).

It is widely acknowledged that hepatic *de novo* lipogenesis (DNL), rather than the uptake of circulating free fatty acids (FFAs), impaired lipid β-oxidation, or decreased VLDL secretion, is a major contributor to the excess lipids and hepatic steatosis in various contexts (such as obesity and high-carbohydrate diet) (13). A family of enzymes precisely drive the newly synthesized lipids using non-fat materials like carbohydrates in DNL under various dietary situations. Transcription factors like SREBP-1c, LXR, RXR, and ChREBP are thought to play a role in controlling the expression of DNL-associated enzymes like FASN, SCD1, and ACCCA within the intricate molecular regulatory networks controlling the hepatic DNL. Although a lot of study has gone into understanding the regulatory networks, the

fundamental molecular mechanisms that control hepatic DNL are still not fully understood (103-107).

In this chapter, we would like to explore how GPR110 regulates the lipid metabolism in the liver. We used hepatic GPR110 overexpression HFD-fed mice model to find the downstream target of GPR110 and try to develop a new strategy for NAFLD therapy.

4.2 Results

4.2.1 SCD1 may be the potential downstream target of GPR110

To reveal the molecular mechanism underlying the involvement of hepatic GPR110 in the progression of NAFLD, we used RNA-sequencing analysis. The RNA samples were extracted from the livers of HFD-fed ASO-NC treated rAAV-GFP, ASO-NC treated rAAV-GPR110 and ASO-GPR110 treated rAAV-GPR110 mice. It is shown that the lipid metabolism is the most relevant pathway in research for metabolisms (Fig. 4.1A). Among these gene, we found that stearoyl CoA desaturase 1 (SCD1) had the largest change among different groups (Fig. 4.1B). To further validate the sequencing data, qPCR was conducted, and the results were in consistence, where SCD1 tended to be the largest changed gene (Fig. 4.1C). SCD1 is reported to be a key lipogenic enzyme that closely related to the lipid metabolism. It is responsible for the rate-limiting step in the synthesis of monounsaturated fatty acids (MUFAs) such as oleate and palmitoleate, by forming double bonds in saturated fatty acids (80). MUFAs act as substrates for the synthesis of various kinds of lipids. Moreover, increased SCD1 activity is revealed to be involved in the development of NAFLD, hypertriglyceridemia and diabetes (81, 82).
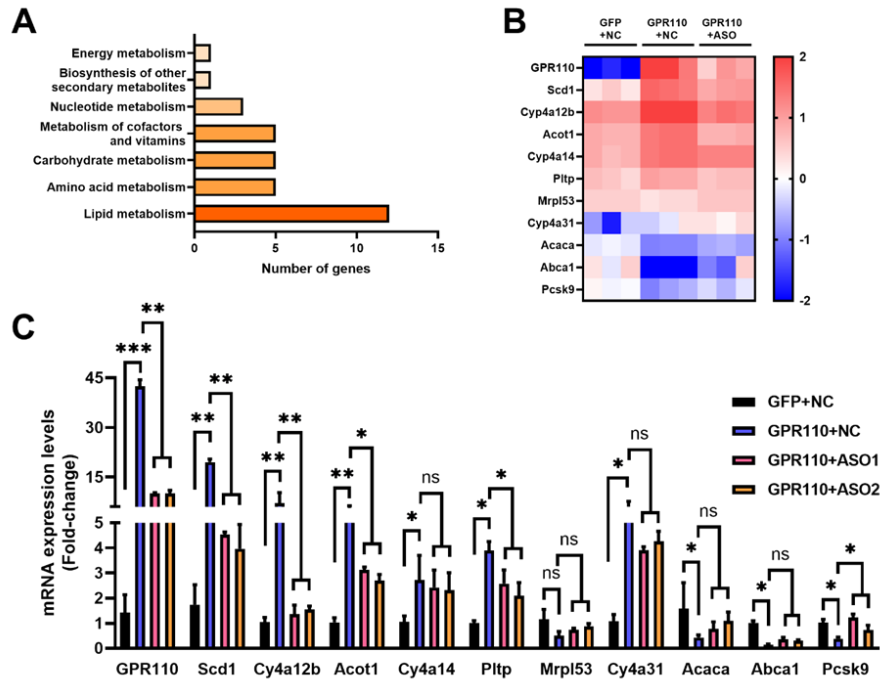
Figure 4.1. SCD1 is a potential downstream target of GPR110 related to the lipid metabolism. Mice were sacrificed and mRNA of liver from each group were extracted for RNA-seq analysis. (A) KEGG pathway assay of differential mRNA transcripts in rAAV and ASO groups identified. (B) Heat map show the log2 scale fold change in the expression levels of a set of genes involved in lipid metabolism from RNA seq data of livers. n=3 per group. (C) mRNA expression levels of genes according to the heatmap from different groups of mice received either GFP-NC, GPR110-NC, GPR110-ASO1 or GPR110-ASO2 fed with HFD, respectively, as determined by qPCR analysis. Data represent as mean ± SEM; n = 8 mice per group; repeated with three independent experiments; P value analyzed by two-tailed Student's *t* test. *P < 0.05, **P < 0.01, ***P < 0.001.

4.2.2 Expression levels of hepatic GPR110 are also correlated to SCD1 expression and severity of hepatosteatosis in humans

To explore the possible clinical relevance of our findings, we also check the expression level of GPR110 in human liver which was a published transcriptome dataset Gene Expression Omnibus (GEO; Profile # GDS4881 / 8126820). The researchers used liver biopsy samples of human from control (healthy) to patients with different phases of NAFLD to do the screening work. In agreement with our findings in animal models, healthy obese subjects without NAFLD have a much lower GPR110 expression level in the liver, but the level of hepatic GPR110 decreased in obese subjects, the degree of decrease was not as dramatic as in mice (Fig. 4.2A). Obese patients who were diagnosed with NAFLD tend to have a higher hepatic expression level. In addition, we also explore the correlation between the expression level of GPR110 and SCD1 in liver (Fig. 4.2B). Interestingly, in agreement with our RNA-seq results, the hepatic SCD1 mRNA levels exhibited a positive association with GPR110 mRNA (r^2=0.4635; p = 0.0044; Fig. 4.2B). Collectively, both human and mice's hepatic GPR110 expression levels were decreased in obese subjects without NAFLD, but its level will increase when NAFLD occurred. Moreover, hepatic SCD1 expression is tightly related to the hepatic expression of GPR110, which gives a hint that SCD1 may be the potential downstream target of GPR110, regulating the lipid metabolism.
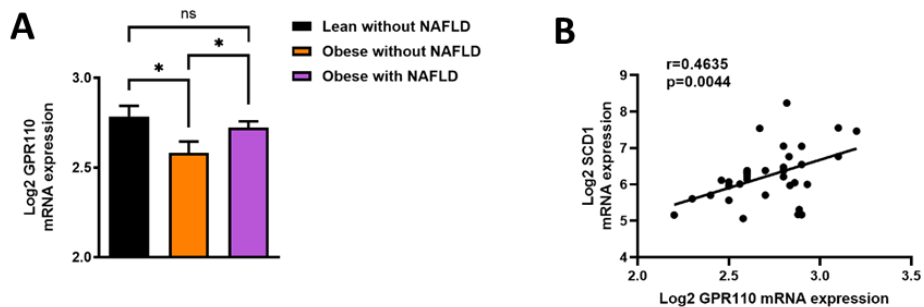
Figure 4.2. Expression level of hepatic GPR110 is also related to the severity of NAFLD and expression of hepatic SCD1 in humans. (A) Normalized Log_2 mRNA expression of GPR110 in lean people without NAFLD (n=12), obese people without NAFLD (n=17) or obese patients with NAFLD (n=8) according to the GEO database (GEO; Profile # GDS4881 / 8126820). (B) Correlation between GPR110 and SCD1 in liver of human subjects based on the GEO database. Data represent as mean ± SEM; n = 8 mice per group; repeated with three independent experiments; P value analyzed by two-tailed Student's *t* test. $*P < 0.05$, $**P < 0.01$, $***P < 0.001$.

4.2.3 The upregulation of SCD1 expression is driven by the presence of GPR110

We conducted *in vitro* assays to confirm SCD1 expression is induced by GPR110, by using adenovirus mediated GPR110 expression system (ADV-GPR110) to overexpress GPR110 in primary hepatocytes isolated from STC-fed mice. Similar to the animal experiments, after infection, the ASO-GPR110s were added to knockdown the expression of GPR110 in ADV-infected primary hepatocytes. The expression level of SCD1 was measured. qPCR analysis indicated that SCD1 mRNA level was significantly increased in primary hepatocytes infected with ADV-GPR110 but not ADV-GFP (Fig. 4.3A). Western blot experiment of SCD1 protein also revealed a similar pattern (Fig. 4.3B).
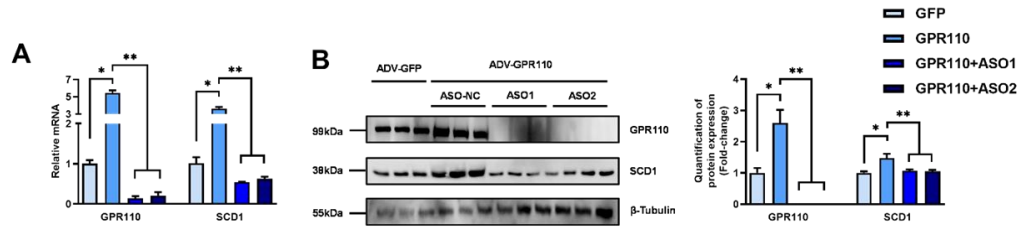
Figure 4.3. SCD1 expression is regulated by GPR110 in primary hepatocytes. (A) Primary hepatocytes were infected with either adenoviral vector expressing GPR110 (ADV-GPR110) or control adenovirus expressing GFP (ADV-GFP) 24h after plating, followed by transfection with ASO1-GPR110, ASO2-GPR110 or ASO-NC for another 6 hours. mRNA expression levels of GPR110 and SCD1 from different groups were assessed, as determined by qPCR analysis. (B) Immunoblotting analysis for the expression level of GPR110 and SCD1 from different groups of primary hepatocytes. Each lane is a sample from a different plate. Data represent as mean ± SEM; n = 8 mice per group; repeated with three independent experiments; P value analyzed by two-tailed Student's *t* test. *P < 0.05, **P < 0.01, ***P < 0.001.

4.2.1 Cellular lipid abundance is correlated to the expression level of GPR110

We also measured the lipid content of the primary hepatocytes infected with ADV and ASO. Consistent with our *in vivo* observations, we found that overexpression of GPR110 increased the intracellular CHO (Fig. 4.4A), TG (Fig. 4.4B) and FFA (Fig. 4.4C). These results were similar with the lipid pattern where primary hepatocytes were treated with rAAV-GPR110 and shSCD1 to repress the expression level of SCD1 (Fig. 4.4A-C). Collectively, the increases of lipid contents may be partially repressed by overexpressing SCD1 specific shRNAs and completely repressed by ASO against GPR110.
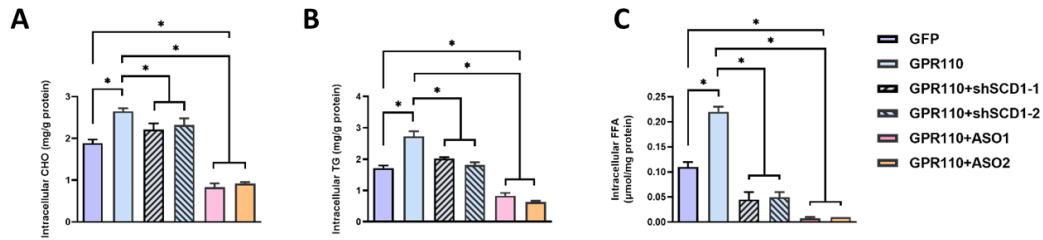
Figure 4.4. Cellular lipid abundance is closely correlated to GPR110 expression. (C) Primary hepatocytes were infected with either adenoviral vector expressing GPR110 (ADV-GPR110) or control adenovirus expressing GFP (ADV-GFP), followed by transfecting with scramble or shSCD1-1 or shSCD1-2 plasmids for another 72 hours. Intracellular lipids were extracted and CHO (C), TG (D), and FFA (E) were assessed. Data represent as mean ± SEM; n = 8 mice per group; repeated with three independent experiments; P value analyzed by two-tailed Student's *t* test. *P < 0.05, **P < 0.01, ***P < 0.001.

4.2.2 Luciferase reporter assay confirms that SCD1 is a downstream target of GPR110

To further validate that the expression of SCD1 was transcriptional regulated by GPR110, *in vitro* luciferase reporter assays were conducted. We first constructed plasmid harbouring luciferase gene driven by the mouse SCD1 promoter (-2000 to +100) in pGL3-basic backbone. This plasmid was then transfected into HEK293 cells. On the other hand, since previous study demonstrated that DHEA was a ligand of GPR110 (79), we here used DHEA to activate the activity of GPR110 in the cell lines. It is found that there was no change of luciferase activity of pGL3-SCD1 promoter-Luciferase transfected HEK293 cells to the treatment of GPR110 ligand unless the cells were pre-infected with ADV-GPR110 for the overexpression (Fig. 4.5A). Thus, it can be concluded that the transcription level of SCD1 is regulated by GPR110. Additionally, no differences can be observed in the mRNA expression of GPR110 and SCD1 in HEK293 cells infected with ADV-GFP. But the expression of these two genes were increased after ADV-GPR110 infection. It is shown that the highest SCD1 mRNA was found under the condition which treated with both ADV-GPR110 and DHEA (Fig. 4.5B).
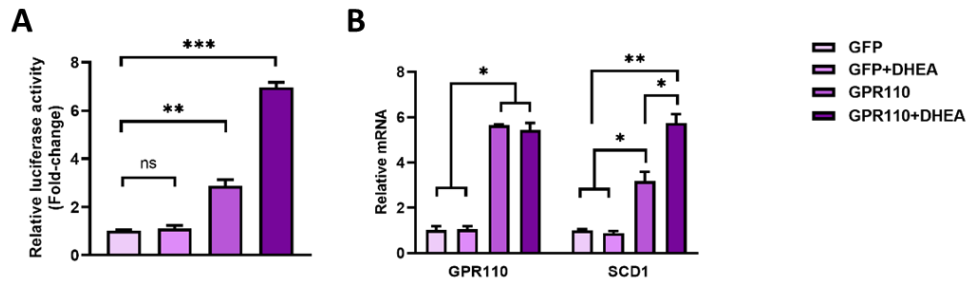
Figure 4.5. SCD1 expression is the downstream target of GPR110 by a luciferase reporter assay. (A) HEK293 cells were infected with pGL3-SCD1 promoter-luciferase plasmid and adenoviral vector expressing GPR110 (ADV-GPR110) or GFP (ADV-GFP) for 24 h and DHEA was added to the transfected cells at the concentration of 100 μM for 48 h. Cell lysates were used for luciferase assay. Lysates from the cell co-transfection with pGL3-SCD1 promoter-luciferase plasmid and ADV-GFP without treatment of DHEA was set as 1 for fold-change calculation. (B) HEK293 cells were infected with adenoviral vector expressing either GPR110 (ADV-GPR110) or GFP (ADV-GFP) for 24 h and DHEA was added to the infected cells at the concentration of 100 μM for 48 h. Cells were harvested and mRNA expression levels of GPR110 and SCD1 were determined by qPCR analysis. Data represent as mean ± SEM; n = 8 mice per group; repeated with three independent experiments; P value analyzed by two-tailed Student's *t* test. *P < 0.05, **P < 0.01, ***P < 0.001.

4.2.3 Inhibition of SCD1 in rAAV-GPR110 mice attenuates the severity of obesity in rAAV-GPR110 mice

To examine whether the up-regulation of hepatic SCD1 expression is the reason that leads to the metabolic dysregulation in rAAV-GPR110 obese mice, a liver-specific SCD1 inhibitor MK8245 was used and given to the hepatic GPR110 overexpression mice (Fig. 4.6A) (108, 109). Chronic treatment of MK8245 for 11 weeks will not affect the expression of GPR110 mRNA (Fig. 4.6B) as well as the protein level (Fig. 4.6C) in rAAV-GPR110 mice.

Similar to previous studies which illustrated that the chronic treatment of MK8245 will improve different metabolic parameters (108), we found that the treatment of SCD1 inhibitor lowered the body weight (Fig. 4.7A), improved glucose homeostasis including fasting blood glucose level (Fig. 4.7B), fasting insulin level (Fig. 4.7C) and HOMA-IR (Fig. 4.7D). The improved glucose metabolic ability was also showed in GTT (Fig. 4.7E) and PTT (Fig. 4.7F) when compared to the untreated littermates. There remained no difference detected in insulin sensitivity according to the result of ITT (Fig. 4.7G).
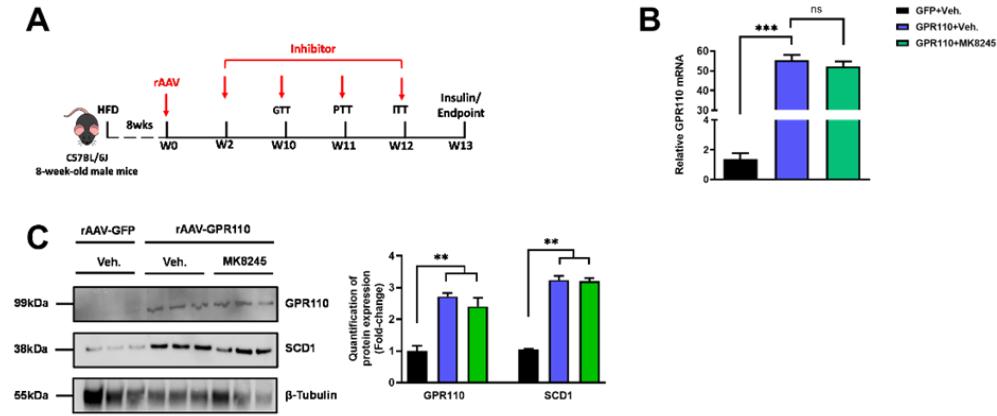
Figure 4.6. Inhibition of SCD1 will not affect the hepatic GPR110 expression. (A) Schematic illustration of viral treatments. (B) Hepatic mRNA expression levels of GPR110 from different groups of mice received rAAV and inhibitor fed with HFD respectively, as determined by qPCR analysis. (C) Immunoblotting analysis for the hepatic protein expression level of GPR110 and SCD1 from different groups of mice fed with HFD. Each lane is a sample from a different individual. Data represent as mean ± SEM; n = 8 mice per group; repeated with three independent experiments; P value analyzed by two-tailed Student's *t* test. *P < 0.05, **P < 0.01, ***P < 0.001.
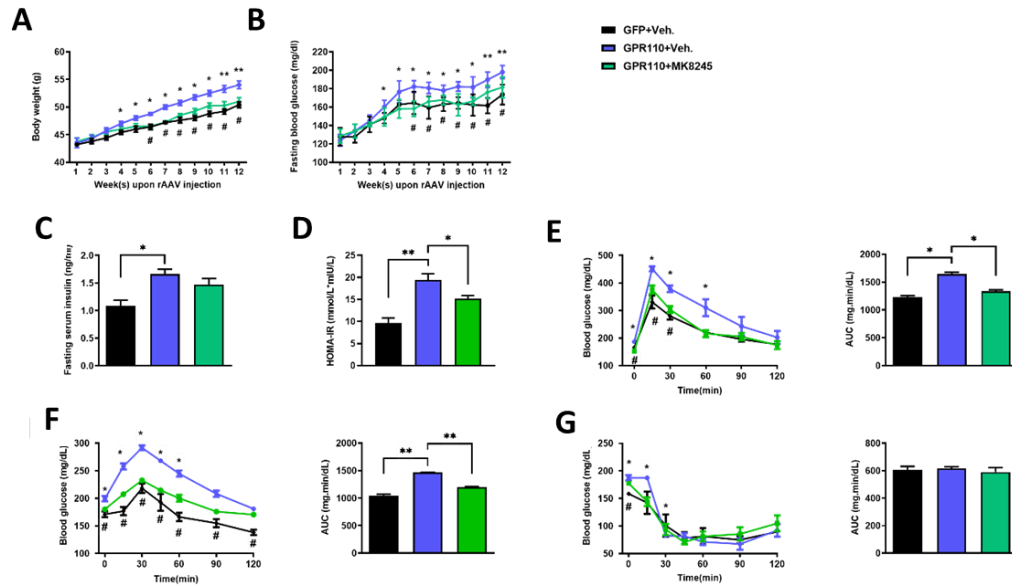
Figure 4.7. SCD1 inhibition alleviates the glucose impairment in mice with hepatic GPR110 overexpression. (A) Body weight and (B) fasting blood glucose level were measured. (C) The fasting blood insulin level and (D) HOMA-IR index were measured and calculated at the end of the experiment. (E) GTT (1g/kg BW, left) and AUC (right) of serum glucose at the week of 10. (F) PTT (1g/kg BW, left) and AUC (right) of serum glucose at week 11. (G) ITT (0.5 U/kg BW, left) and AUC (right) of serum glucose at week of 12. Data represent as mean ± SEM; n = 8 mice per group; repeated with three independent experiments; P value analyzed by two-tailed Student's *t* test. *P < 0.05, **P < 0.01, ***P < 0.001.

4.2.4 Treatment with the SCD1 inhibitor in rAAV-GPR110 mice lowers the circulating lipid levels

Besides, MK8245 treatment also improved the circulating lipid profile including CHO (Fig. 4.8A) and TG (Fig. 4.8B) to almost the level of rAAV-GFP littermates. FFA remained no difference among these groups (Fig. 4.8C). Even though a relatively higher HDL can be found in the SCD1 inhibition group but there was no difference regarding the level of LDL (Fig. 4.8 D). Moreover, the degree of liver damage was also alleviated as the liver enzymes AST and ALT level were decreased in the inhibitor group compared to the overexpression one (Fig. 4.8E). To conclude, treating SCD1 inhibitor MK8245 improved the lipid profile as well as the severity of liver damage in GPR110 overexpression group.

4.2.5 Hepatic SCD1 inhibition alleviates the severity of hepatic steatosis in GPR110-overexpressing mice

In terms of the hepatic lipid accumulation, we found that the inhibitor treatment group showed a lower liver/body weight ratio compared to the rAAV-GPR110 group (Fig. 4.9A). This result can also be observed in the H&E as well as Oil Red O staining, showing that the rAAV-GPR110 had a highest lipid content in the liver but the severity was improved after MK8245 treatment (Fig. 4.9B).

Finally, we measured the hepatic lipid content in mice. Similarly, the content of CHO (Fig. 4.10A), TG (Fig. 4.10B) and FFA (Fig. 4.10C) decreased in the SCD1 inhibition group. To conclude, chronic treatment of SCD1 inhibitor MK8245 will partially alleviated the lipid accumulations in the liver.
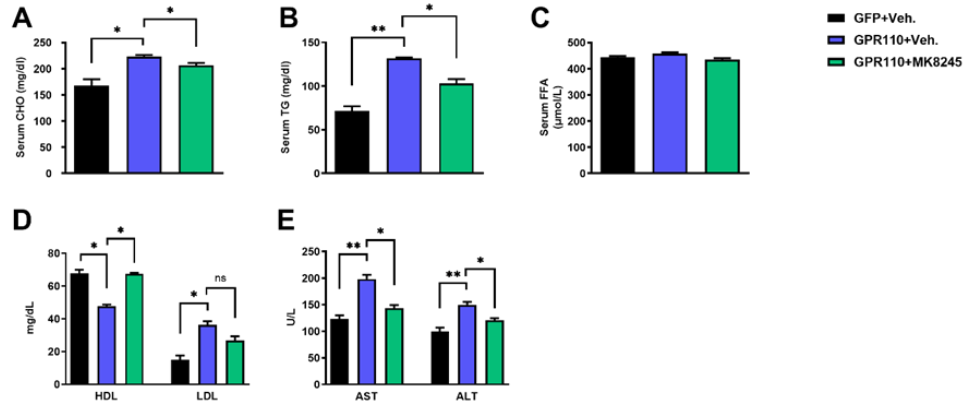
Figure 4.8. Inhibiting hepatic SCD1 alleviates the severity of lipid accumulation in GPR110 overexpression mice. (A) Serum CHO, (B) serum TGs and (C) serum FFA levels at the end of experiment. (D) Serum HDL and LDL, (E) AST and ALT level of each group of mice were measured at the end of the experiment. Data represent as mean ± SEM; n = 8 mice per group; repeated with three independent experiments; P value analyzed by two-tailed Student's *t* test. *P < 0.05, **P < 0.01, ***P < 0.001.
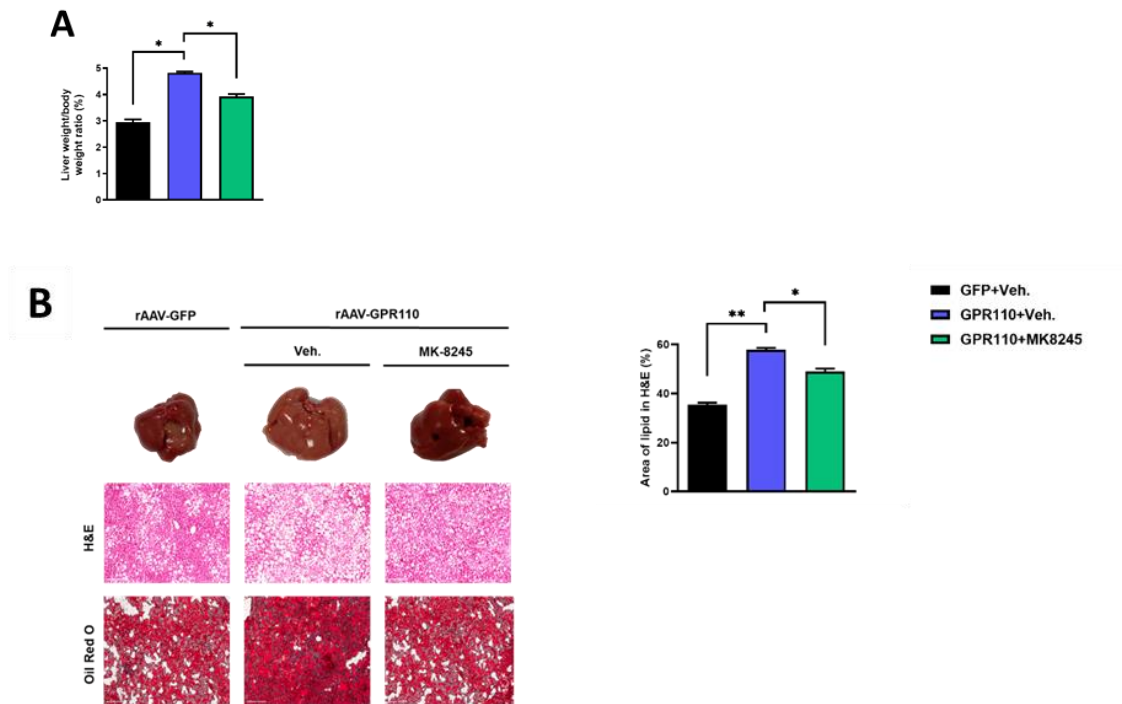
Figure 4.9. Hepatic SCD1 inhibition alleviates the severity of hepatic steatosis in GPR110 overexpression mice. (A) The ratio of the liver weight against body weight were calculated after sacrificing the mice from four different groups. (B) Representative gross pictures of liver tissues (upper panels), representative images of H&E (middle panels) and Oil Red O (lower panels) staining of liver sections (200µm). The percentage of lipid area according to H&E staining (right panel. Data represent as mean ± SEM; n = 8 mice per group; repeated with three independent experiments; P value analyzed by two-tailed Student's *t* test. *P < 0.05, **P < 0.01, ***P < 0.001.
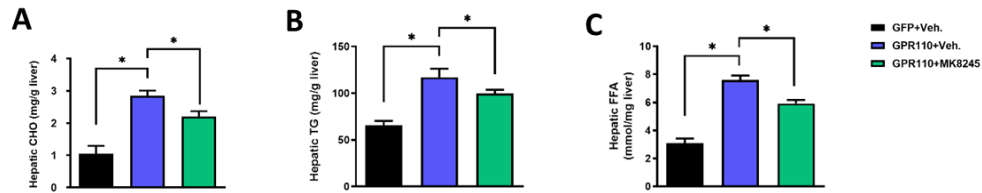
Figure 4.10. Inhibition of hepatic SCD1 prevents the over-accumulation of hepatic lipids in rAAV-GPR110 mice. (A) Hepatic CHO, (B) hepatic TGs and (C) hepatic FFA were normalized by the weight of liver samples used for lipid extraction. Data represent as mean ± SEM; n = 8 mice per group; repeated with three independent experiments; P value analyzed by two-tailed Student's *t* test. *P < 0.05, **P < 0.01, ***P < 0.001.

4.3 Summary

In this chapter, we aimed to explore the downstream target of GPR110. Therefore, we first used RNA-sequencing to screen the genes that may potentially be relevant to the GPR110 from either rAAV-GFP or rAAV-GPR110 treated with ASO-GPR110 or ASO-NC group. It is found that lipid metabolism had the most genes involved in and among them, SCD1 had the highest variation. SCD1 is known to be the key gene which regulate the lipid metabolism in animal models. Given the hypothesis that SCD1 may be the downstream target of GPR110, we first used *in vitro* assay to prove that the expression of SCD1 is closely related to the level of GPR110. And the luciferase reporter assays also revealed that the transcriptional level of SCD1 is regulated by the expression and the activation of GPR110. Therefore, we used the liver specific SCD1 (MK8245) to inhibit its function in hepatic GPR110 overexpression mice. As expect, chronic treatment of SCD1 inhibitor leaded to a better metabolism ability in GPR110 overexpression mice, especially improved the hepatic lipid accumulation. Treating SCD1 inhibitor had a similar effect with ASO-GPR110s, demonstrating that the compensated effect of ASO-GPR110 may be due to the lower expression and activity of SCD1 in the liver.

To conclude, SCD1 is a downstream target of GPR110, which regulates the lipid metabolism in the liver.

Chapter 5 - General discussion

5.1 GPR110 expression is closely related to a metabolic disorder in the liver

In this study, we reported a correlation between a novel GPCR – GPR110 and liver steatosis in mice and human. The published studies of GPR110 now are mainly focus on its immunological function, no article aimed to explore its role in metabolism. We are the first to demonstrated that GPR110 is required for regulating lipid content in liver in the DIO mice by both gaining and losing function approaches.

Briefly, by overexpression of hepatic GPR110 level, the HFD-induced steatosis and liver injury will be promoted in DIO mice. ASO was used to knockdown the hepatic expression of GPR110 as the sequences we used were N-acetylgalactaosamine (GaINAc) conjugated, which may bind to the regions of GPR110 mRNA to suppress its expression. Moreover, since liver hepatocytes has abundant and exclusive expression of asialoglycoprotein receptors, which are able to bind and uptake the circulating glycosylated oligonucleotides by receptor-mediated endocytosis (110), the knockdown effect can be regarded as liver specific. After chronic treatment of ASO-GPR110, the obese-induced NAFLD was alleviated in rAAV-GPR110 mice. We thus hypothesized the downregulation of hepatic GPR110 expression level in obese subjects may play a protective role to prevent the excessive fat accumulation in the liver.

5.2 GPR110 regulates the lipid metabolism by upregulating the hepatic expression of SCD1

To decipher the underlying mechanism how GPR110 regulates the lipid metabolism in the liver, we conducted RNA-sequencing analysis and found that SCD1 had the highest correlation of GPR110. It is reported that SCD1 is an enzyme located in the endoplasmic reticulum and is responsible for the catalysation in the formation of MUFAs by adding a double bond (111). SCD1 had a crucial role in metabolism as it is found that the global knockout mice of SCD1 are lean and protected against from both diet-induced and genetic driven obesity (49, 50, 112). Moreover, liver-specific knockout of SCD1 in high-carbohydrate diet induced adiposity mice indicated a reduced level of hepatic lipogenesis and improved glucose tolerance (51). Therefore, to prove that the change of metabolic phenotype changes in rAAV-GPR110 mice was due to the increase expression of SCD1 in the liver, we used liver specific SCD1 inhibitor to repress its function. Concordantly, pharmacologically inhibiting SCD1 was sufficient to rescue the key metabolic disorders in GPR110 overexpression mice without changing its hepatic expression. Thus, we draw the conclusion that GPR110 induces SCD1 expression, resulting in the increase of *de novo* lipogenesis in liver as well as exacerbating the obese-induced NAFLD.

Based on previous research obtained from SCD1 knockout mice, the inhibition of SCD1 was proposed to be a novel strategy for metabolic syndrome therapy (113). However, the expression level of SCD1 is tightly

97

regulated and inhibition of SCD1 will cause a serious harmful consequences such as proinflammatory and endoplasmic reticulum stress by the accumulation of SCD1 substrates (114, 115). For this reason, optimal level of SCD1 is required to maintain health. On the other hand, based on our findings, either the dispensable of GPR110 in adult mice of GPR110 knockout mice or dramatical reduction GPR110 shown no harmful phenotypes. Moreover, shown no harmful phenotypes. Moreover, recent study also demonstrated that the deficiency of GPR110 will decelerate the carcinogen-induced hepatocarcinogenesis in adult mice (95). Therefore, targeting hepatic GPR110 is a potential safe treatment of NAFLD.

5.3   Limitations of this study

Although in this research, we unmasked the relationship between GPR110 and SCD1, in the regulation of lipid metabolism in both human and diet-induced obese animal models. However, different types of animal models (ob/ob or db/db mice) need to be used to identify whether in these gene-mutated obese mice also shown the similar results. Another limitation is that although the ASO sequences we used in this study have higher affinity to bind the hepatocytes in the liver, there may still have some off-target effect which mean it may also knockdown the expression of other tissues and consequently have the influence on the metabolism.

5.4   Conclusion and future directions

To conclude, this study has uncovered a novel function of GPR110 in regulating hepatic lipid metabolism and revealed its mechanism which is at least in part achieved through the regulation of SCD1 expression levels (Fig. 5.1A). In chapter 3, I have first uncovered the expression pattern of GPR110 and explored its metabolic function in the liver by both gain-of-function and loss-of-function studies. It is found that the severity of obesity and lipid accumulation were increased in mice with rAAV-mediated overexpression of GPR110. The relevant metabolic features and the metabolic functions were improved after ASO-mediated knockdown of the hepatic expression level of GPR110. In chapter 4, I have identified a downstream target of GPR110 in the liver by RNA-sequencing. Both *in vitro* and *in vivo* experiments consistently illustrated that GPR110 regulates the lipid metabolism by regulating the expression levels of SCD1. Briefly, ADV was employed to overexpress GPR110 in primary hepatocytes, followed by treatment with either ASO or shSCD1. The SCD1 expression levels and the intracellular lipids were measured. Moreover, a liver-specific SCD1 inhibitor was adopted to inhibit the function of SCD1 in GPR110-overexpressing mice. In these mice, the metabolic disorders were attenuated, a similar effect that could be achieved after treatment with ASO-GPR110. Hence, my findings demonstrated that GPR110 may serve as a potential therapeutic candidate for the treatment of NAFLD.

One recent study has reported that N-docosahexaenoylethanolamine (DHEA, also named as synaptamide) is one of the endogenous ligands of GPR110 (79). On the other hand, DHEA is also identified as a ligand which stimulates the endocannabinoid receptor CB_1R in liver, promoting the synthesis of lipids by inducing SCD1 expression (116, 117). In contrast to the repressed expression levels of GPR110 in the liver in obese subjects, the expression of hepatic cannabinoid is highly upregulated in obesity (117). Therefore, it is interesting to explore whether GPR110 can regulate the DHEA-induced SCD1 expression by cooperating with CB_1R.

In addition, as mentioned above, other studies on GPR110 have mainly focused on its role in cancer by identifying it as an oncogene (75, 95, 118-123). Coincidently, people with high expression levels of SCD1 are also genetically susceptible to hepatocarcinogenesis (124). Based on the corelation we reported in this study, it is highly possible that GPR110 accelerates carcinogenesis by inducing SCD1 expression. In response to this hypothesis, further experiments are warranted to check the SCD1 expression levels in GPR110-induced cancers.

In summary, in this thesis work, I provide the first evidence to demonstrate that the physiological function of GPR110 is for modulation of hepatic lipid metabolism via SCD1 expression. Down-regulation of GPR110 expression in obese subjects acts as a protective mechanism for preventing over-accumulation of lipid in the liver. As a result, blocking GPR110 is an effective therapeutic approach for the treatment of NAFLD.
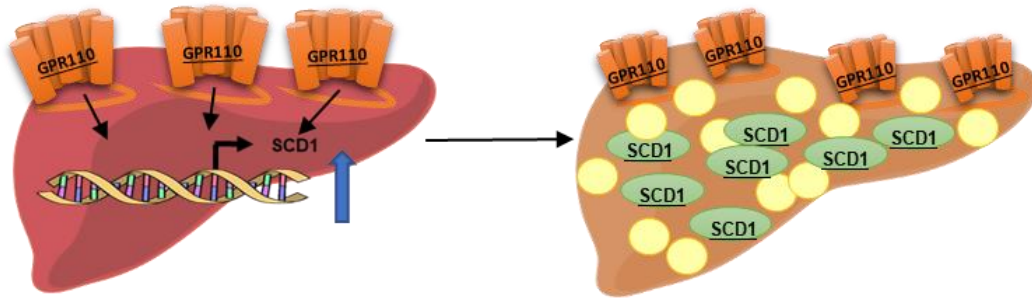
Figure 5.1. GPR110 regulates the lipid metabolism in liver by upregulating the expression of SCD1. The expression level of GPR110 is tightly correlated to the nutritional status of the subjects and the level will decrease in obese subjects. Overexpression of hepatic GPR110 will lead to lipid accumulation in the liver via up-regulating the SCD1 expression, leading to NAFLD.

References

1.   Wyatt SB, Winters KP, Dubbert PM. Overweight and obesity: prevalence, consequences, and causes of a growing public health problem. The American journal of the medical sciences. 2006;331(4):166-74.

2.   Wilborn C, Beckham J, Campbell B, Harvey T, Galbreath M, La Bounty P, et al. Obesity: prevalence, theories, medical consequences, management, and research directions. Journal of the International Society of Sports Nutrition. 2005;2(2):4.

3.   Seidell JC, Flegal KM. Assessing obesity: classification and epidemiology. British medical bulletin. 1997;53(2):238-52.

4.   Colditz GA. Economic costs of obesity and inactivity. Medicine and science in sports and exercise. 1999;31(11 Suppl):S663-7.

5.   Finkelstein EA, Fiebelkorn IC, Wang G. National Medical Spending Attributable To Overweight And Obesity: How Much, And Who's Paying? Further evidence that overweight and obesity are contributing to the nation's health care bill at a growing rate. Health affairs. 2003;22(Suppl1):W3-219-W3-26.

6.   Murphy C, Yates J. Economic comparison of weight loss programmes versus drug treatment for the management of obesity. Asia Pacific Journal of Clinical Nutrition. 2005;14:97-105.

7.   Werner M, Driftmann S, Kleinehr K, Kaiser GM, Mathé Z, Treckmann JW, et al. All-In-One: Advanced preparation of Human Parenchymal and Non-Parenchymal Liver Cells. PloS one. 2015;10(9):e0138655.

8.   Thompson D, Brown JB, Nichols GA, Elmer PJ, Oster G. Body mass index and future healthcare costs: a retrospective cohort study. Obesity Research. 2001;9(3):210-8.

9.   Targher G, Day CP, Bonora E. Risk of cardiovascular disease in patients with nonalcoholic fatty liver disease. New England Journal of Medicine. 2010;363(14):1341-50.

10.   Angulo P. Nonalcoholic fatty liver disease. New England Journal of Medicine. 2002;346(16):1221-31.

11.   Savage DB, Petersen KF, Shulman GI. Disordered lipid metabolism and the pathogenesis of insulin resistance. Physiological reviews. 2007;87(2):507-20.

12.   Hu FB, Manson JE, Stampfer MJ, Colditz G, Liu S, Solomon CG, et al. Diet, lifestyle, and the risk of type 2 diabetes mellitus in women. New England journal of medicine. 2001;345(11):790-7.

13.   Fabbrini E, Sullivan S, Klein S. Obesity and nonalcoholic fatty liver disease: biochemical, metabolic, and clinical implications. Hepatology. 2010;51(2):679-89.

14.   Marchesini G, Bugianesi E, Forlani G, Cerrelli F, Lenzi M, Manini R, et al. Nonalcoholic fatty liver, steatohepatitis, and the metabolic syndrome. Hepatology. 2003;37(4):917-23.

15.   Kleiner DE, Brunt EM, Van Natta M, Behling C, Contos MJ, Cummings OW, et al. Design and validation of a histological scoring system for nonalcoholic fatty liver disease. Hepatology. 2005;41(6):1313-21.

16.   Ludwig J, Viggiano TR, Mcgill DB, Oh B, editors. Nonalcoholic steatohepatitis: Mayo Clinic experiences with a hitherto unnamed disease. Mayo Clinic Proceedings; 1980.

17.   Adler M, Schaffner F. Fatty liver hepatitis and cirrhosis in obese patients. The American journal of medicine. 1979;67(5):811-6.

18.   Powell EE, Cooksley WGE, Hanson R, Searle J, Halliday JW, Powell W. The natural history of nonalcoholic steatohepatitis: a follow-up study of forty-two patients for up to 21 years. Hepatology. 1990;11(1):74-80.

19.   Ratziu V, Giral P, Charlotte F, Bruckert E, Thibault V, Theodorou I, et al. Liver fibrosis in overweight patients. Gastroenterology. 2000;118(6):1117-23.

20.   Clark JM, Brancati FL, Diehl AME. Nonalcoholic fatty liver disease: the most common cause of abnormal liver enzymes in the US population. Gastroenterology. 2001;5(120):A65.

21.   Hilden M, Christoffersen P, Juhl E, Dalgaard J. Liver histology in a 'normal'population—examinations of 503 consecutive fatal traffic casualties. Scandinavian journal of gastroenterology. 1977;12(5):593-7.

22.   Lee RG. Nonalcoholic steatohepatitis: a study of 49 patients. Human pathology. 1989;20(6):594-8.

23.   Gholam PM, Kotler DP, Flancbaum LJ. Liver pathology in morbidly obese patients undergoing Roux-en-Y gastric bypass surgery. Obesity Surgery. 2002;12(1):49-51.

24.   Romeo S, Kozlitina J, Xing C, Pertsemlidis A, Cox D, Pennacchio LA, et al. Genetic variation in PNPLA3 confers susceptibility to nonalcoholic fatty liver disease. Nature genetics. 2008;40(12):1461-5.

25.   Browning JD, Szczepaniak LS, Dobbins R, Nuremberg P, Horton JD, Cohen JC, et al. Prevalence of hepatic steatosis in an urban population in the United States: impact of ethnicity. Hepatology. 2004;40(6):1387-95.

26.   Rui L. Energy metabolism in the liver. Comprehensive physiology. 2014;4(1):177.

27.   Racanelli V, Rehermann B. The liver as an immunological organ. Hepatology. 2006;43(S1):S54-S62.

28.   Agius L. Glucokinase and molecular aspects of liver glycogen metabolism. Biochemical Journal. 2008;414(1):1-18.

29.   Stanley S, Pinto S, Segal J, Pérez CA, Viale A, DeFalco J, et al. Identification of neuronal subpopulations that project from hypothalamus to both liver and adipose tissue polysynaptically. Proceedings of the National Academy of Sciences. 2010;107(15):7024-9.

30.   Gerner RR, Wieser V, Moschen AR, Tilg H. Metabolic inflammation: role of cytokines in the crosstalk between adipose tissue and liver. Canadian journal of physiology and pharmacology. 2013;91(11):867-72.

31.   Romacho T, Elsen M, Röhrborn D, Eckel J. Adipose tissue and its role in organ crosstalk. Acta physiologica. 2014;210(4):733-53.

32.   Hugo SE, Cruz-Garcia L, Karanth S, Anderson RM, Stainier DY, Schlegel A. A monocarboxylate transporter required for hepatocyte secretion of ketone bodies during fasting. Genes & development. 2012;26(3):282-93.

33.   Samuel VT, Shulman GI. Mechanisms for insulin resistance: common threads and missing links. Cell. 2012;148(5):852-71.

34.   Seyer P, Vallois D, Poitry-Yamate C, Schütz F, Metref S, Tarussio D, et al. Hepatic glucose sensing is required to preserve β cell glucose competence. The Journal of clinical investigation. 2013;123(4):1662-76.

35.   Van Schaftingen E, Gerin I. The glucose-6-phosphatase system. Biochemical Journal. 2002;362(3):513-32.

36.   Yang C, Ko B, Hensley CT, Jiang L, Wasti AT, Kim J, et al. Glutamine oxidation maintains the TCA cycle and cell survival during impaired mitochondrial pyruvate transport. Molecular cell. 2014;56(3):414-24.

37.   Jitrapakdee S, Wallace JC. Structure, function and regulation of pyruvate carboxylase. Biochemical Journal. 1999;340(1):1-16.

38.   Dias J, Alvarez M, Diez A, Arzel J, Corraze G, Bautista J, et al. Regulation of hepatic lipogenesis by dietary protein/energy in juvenile European seabass (Dicentrarchus labrax). Aquaculture. 1998;161(1-4):169-86.

39.   Wu G, Huang H, Abreu JG, He X. Inhibition of GSK3 phosphorylation of β-catenin via phosphorylated PPPSPXS motifs of Wnt coreceptor LRP6. PloS one. 2009;4(3):e4926.

40.   Jelen S, Gena P, Lebeck J, Rojek A, Praetorius J, Frøkiaer J, et al. Aquaporin-9 and urea transporter-A gene deletions affect urea transmembrane passage in murine hepatocytes. American Journal of Physiology-Gastrointestinal and Liver Physiology. 2012;303(11):G1279-G87.

41.   She P, Shiota M, Shelton KD, Chalkley R, Postic C, Magnuson MA. Phosphoenolpyruvate carboxykinase is necessary for the integration of hepatic energy metabolism. Molecular and cellular biology. 2000;20(17):6508-17.

42.   She P, Burgess SC, Shiota M, Flakoll P, Donahue EP, Malloy CR, et al. Mechanisms by which liver-specific PEPCK knockout mice preserve euglycemia during starvation. Diabetes. 2003;52(7):1649-54.

43.   Wagenmakers AJ, Frayn KN, Arner P, Yki-Järvinen H. Fatty acid metabolism in adipose tissue, muscle and liver in health and disease. Essays in biochemistry. 2006;42:89-103.

44.   Cooper AD. Hepatic uptake of chylomicron remnants. Journal of lipid research. 1997;38(11):2173-92.

45.   Zhou J, Zhai Y, Mu Y, Gong H, Uppal H, Toma D, et al. A novel pregnane X receptor-mediated and sterol regulatory element-binding protein-independent lipogenic pathway. Journal of Biological Chemistry. 2006;281(21):15013-20.

46.   An J, Muoio DM, Shiota M, Fujimoto Y, Cline GW, Shulman GI, et al. Hepatic expression of malonyl-CoA decarboxylase reverses muscle, liver and whole-animal insulin resistance. Nature medicine. 2004;10(3):268-74.

47.   Castro LFC, Tocher DR, Monroig O. Long-chain polyunsaturated fatty acid biosynthesis in chordates: Insights into the evolution of Fads and Elovl gene repertoire. Progress in lipid research. 2016;62:25-40.

48.   Ntambi JM. Regulation of stearoyl-CoA desaturase by polyunsaturated fatty acids and cholesterol. Journal of lipid research. 1999;40(9):1549-58.

49.   Ntambi JM, Miyazaki M, Stoehr JP, Lan H, Kendziorski CM, Yandell BS, et al. Loss of stearoyl–CoA desaturase-1 function protects mice against adiposity. Proceedings of the National Academy of Sciences. 2002;99(17):11482-6.

50.   Cohen P, Miyazaki M, Socci ND, Hagge-Greenberg A, Liedtke W, Soukas AA, et al. Role for stearoyl-CoA desaturase-1 in leptin-mediated weight loss. Science. 2002;297(5579):240-3.

51.   Miyazaki M, Flowers MT, Sampath H, Chu K, Otzelberger C, Liu X, et al. Hepatic stearoyl-CoA desaturase-1 deficiency protects mice from carbohydrate-induced adiposity and hepatic steatosis. Cell metabolism. 2007;6(6):484-96.

52.   Morán-Salvador E, López-Parra M, García-Alonso V, Titos E, Martínez-Clemente M, González-Périz A, et al. Role for PPARγ in obesity-induced hepatic steatosis as determined by hepatocyte- and macrophage-specific conditional knockouts. FASEB journal : official publication of the Federation of American Societies for Experimental Biology. 2011;25(8):2538-50.

53.   Lee YJ, Ko EH, Kim JE, Kim E, Lee H, Choi H, et al. Nuclear receptor PPARγ-regulated monoacylglycerol O-acyltransferase 1 (MGAT1) expression is responsible for the lipid accumulation in diet-induced hepatic steatosis. Proceedings

of the National Academy of Sciences of the United States of America. 2012;109(34):13656-61.

54.   Matsusue K, Kusakabe T, Noguchi T, Takiguchi S, Suzuki T, Yamano S, et al. Hepatic steatosis in leptin-deficient mice is promoted by the PPARgamma target gene Fsp27. Cell Metab. 2008;7(4):302-11.

55.   Gavrilova O, Haluzik M, Matsusue K, Cutson JJ, Johnson L, Dietz KR, et al. Liver peroxisome proliferator-activated receptor γ contributes to hepatic steatosis, triglyceride clearance, and regulation of body fat mass. Journal of Biological Chemistry. 2003;278(36):34268-76.

56.   Matsusue K, Haluzik M, Lambert G, Yim SH, Gavrilova O, Ward JM, et al. Liver-specific disruption of PPARgamma in leptin-deficient mice improves fatty liver but aggravates diabetic phenotypes. J Clin Invest. 2003;111(5):737-47.

57.   Herzig S, Hedrick S, Morantte I, Koo SH, Galimi F, Montminy M. CREB controls hepatic lipid metabolism through nuclear hormone receptor PPAR-gamma. Nature. 2003;426(6963):190-3.

58.   Erion DM, Ignatova ID, Yonemitsu S, Nagai Y, Chatterjee P, Weismann D, et al. Prevention of hepatic steatosis and hepatic insulin resistance by knockdown of cAMP response element-binding protein. Cell Metab. 2009;10(6):499-506.

59.   Parthier C, Reedtz-Runge S, Rudolph R, Stubbs MT. Passing the baton in class B GPCRs: peptide hormone activation via helix induction? Trends in biochemical sciences. 2009;34(6):303-10.

60.   Odoemelam CS, Percival B, Wallis H, Chang M-W, Ahmad Z, Scholey D, et al. G-Protein coupled receptors: structure and function in drug discovery. RSC advances. 2020;10(60):36337-48.

61.   Pal K, Melcher K, Xu HE. Structure and mechanism for recognition of peptide hormones by Class B G-protein-coupled receptors. Acta pharmacologica sinica. 2012;33(3):300-11.

62.   Fredriksson R, Lagerström MC, Höglund PJ, Schiöth HB. Novel human G protein-coupled receptors with long N-terminals containing GPS domains and Ser/Thr-rich regions. FEBS letters. 2002;531(3):407-14.

63.   Lee J-W, Huang BX, Kwon H, Rashid MA, Kharebava G, Desai A, et al. Orphan GPR110 (ADGRF1) targeted by N-docosahexaenoylethanolamine in development of neurons and cognitive function. Nature communications. 2016;7(1):1-16.

64.   Stoveken HM, Hajduczok AG, Xu L, Tall GG. Adhesion G protein-coupled receptors are activated by exposure of a cryptic tethered agonist. Proceedings of the National Academy of Sciences. 2015;112(19):6194-9.

65.   Lebesgue D, Wallukat G, Mijares A, Granier C, Argibay J, Hoebeke J. An agonist-like monoclonal antibody against the human β2-adrenoceptor. European journal of pharmacology. 1998;348(1):123-33.

66.   Demberg LM, Winkler J, Wilde C, Simon K-U, Schön J, Rothemund S, et al. Activation of adhesion G protein-coupled receptors: agonist specificity of Stachel sequence-derived peptides. Journal of Biological Chemistry. 2017;292(11):4383-94.

67.   Oldham WM, Hamm HE. Heterotrimeric G protein activation by G-protein-coupled receptors. Nature reviews Molecular cell biology. 2008;9(1):60-71.

68.   Wacker D, Stevens RC, Roth BL. How ligands illuminate GPCR molecular pharmacology. Cell. 2017;170(3):414-27.

69.   Weis WI, Kobilka BK. The molecular basis of G protein–coupled receptor activation. Annual review of biochemistry. 2018;87:897.

70.   Hoare SR. Mechanisms of peptide and nonpeptide ligand binding to Class B G-protein-coupled receptors. Drug discovery today. 2005;10(6):417-27.

71.   Austyn JM, Gordon S. F4/80, a monoclonal antibody directed specifically against the mouse macrophage. European journal of immunology. 1981;11(10):805-15.

72.   Wan WY, Morris A, Kinnear G, Pearce W, Mok J, Wyss D, et al. Pharmacological characterisation of anti-inflammatory compounds in acute and chronic mouse models of cigarette smoke-induced inflammation. Respir Res. 2010;11:126.

73.   Siu FY, He M, De Graaf C, Han GW, Yang D, Zhang Z, et al. Structure of the human glucagon class B G-protein-coupled receptor. Nature. 2013;499(7459):444-9.

74.   Hwang J-I, Yun S, Moon MJ, Park CR, Seong JY. Molecular evolution of GPCRs: GLP1/GLP1 receptors. Journal of Molecular Endocrinology. 2014;52(3):T15-T27.

75.   Lum AM, Wang BB, Beck-Engeser GB, Li L, Channa N, Wabl M. Orphan receptor GPR110, an oncogene overexpressed in lung and prostate cancer. BMC cancer. 2010;10(1):1-14.

76.   Rask-Andersen M, Almén MS, Schiöth HB. Trends in the exploitation of novel drug targets. Nature reviews Drug discovery. 2011;10(8):579-90.

77.   Bjarnadóttir TK, Fredriksson R, Höglund PJ, Gloriam DE, Lagerström MC, Schiöth HB. The human and mouse repertoire of the adhesion family of G-protein-coupled receptors. Genomics. 2004;84(1):23-33.

78.   Bjarnadóttir TK, Geirardsdóttir K, Ingemansson M, Mirza MA, Fredriksson R, Schiöth HB. Identification of novel splice variants of Adhesion G protein-coupled receptors. Gene. 2007;387(1-2):38-48.

79. Lee JW, Huang BX, Kwon H, Rashid MA, Kharebava G, Desai A, et al. Orphan GPR110 (ADGRF1) targeted by N-docosahexaenoylethanolamine in development of neurons and cognitive function. Nature communications. 2016;7:13123.

80. Paton CM, Ntambi JM. Biochemical and physiological function of stearoyl-CoA desaturase. American Journal of Physiology-Endocrinology and Metabolism. 2009;297(1):E28-E37.

81. Kotronen A, Seppänen-Laakso T, Westerbacka J, Kiviluoto T, Arola J, Ruskeepaa A-L, et al. Hepatic stearoyl-CoA desaturase (SCD)-1 activity and diacylglycerol but not ceramide concentrations are increased in the nonalcoholic human fatty liver. Diabetes. 2009;58(1):203-8.

82. Mar-Heyming R, Miyazaki M, Weissglas-Volkov D, Kolaitis NA, Sadaat N, Plaisier C, et al. Association of stearoyl-CoA desaturase 1 activity with familial combined hyperlipidemia. Arteriosclerosis, thrombosis, and vascular biology. 2008;28(6):1193-9.

83. Bale SS, Geerts S, Jindal R, Yarmush ML. Isolation and co-culture of rat parenchymal and non-parenchymal liver cells to evaluate cellular interactions and response. Scientific reports. 2016;6(1):1-10.

84. Xu L, Huang Z, Lo T-h, Lee JTH, Yang R, Yan X, et al. Hepatic PRMT1 ameliorates diet-induced hepatic steatosis via induction of PGC1α. Theranostics. 2022;12(6):2502.

85. Cheng KK, Iglesias MA, Lam KS, Wang Y, Sweeney G, Zhu W, et al. APPL1 potentiates insulin-mediated inhibition of hepatic glucose production and alleviates diabetes via Akt activation in mice. Cell Metabolism. 2009;9(5):417-27.

86.   Younossi ZM, Koenig AB, Abdelatif D, Fazel Y, Henry L, Wymer M. Global epidemiology of nonalcoholic fatty liver disease—meta-analytic assessment of prevalence, incidence, and outcomes. Hepatology. 2016;64(1):73-84.

87.   Peng C, Stewart AG, Woodman OL, Ritchie RH, Qin CX. Non-alcoholic steatohepatitis: a review of its mechanism, models and medical treatments. Frontiers in Pharmacology. 2020;11:603926.

88.   Rinella ME, Sanyal AJ. Management of NAFLD: a stage-based approach. Nature reviews Gastroenterology & hepatology. 2016;13(4):196-205.

89.   Allen AM, Hicks SB, Mara KC, Larson JJ, Therneau TM. The risk of incident extrahepatic cancers is higher in non-alcoholic fatty liver disease than obesity–a longitudinal cohort study. Journal of hepatology. 2019;71(6):1229-36.

90.   Zhou F, Zhou J, Wang W, Zhang XJ, Ji YX, Zhang P, et al. Unexpected rapid increase in the burden of NAFLD in China from 2008 to 2018: a systematic review and meta-analysis. Hepatology. 2019;70(4):1119-33.

91.   Reimer KC, Wree A, Roderburg C, Tacke F. New drugs for NAFLD: lessons from basic models to the clinic. Hepatology international. 2020;14(1):8-23.

92.   Sriram K, Insel PA. G protein-coupled receptors as targets for approved drugs: how many targets and how many drugs? Molecular pharmacology. 2018;93(4):251-8.

93.   Kurtz R, Anderman MF, Shepard BD. GPCRs get fatty: The role of G protein-coupled receptor signaling in the development and progression of nonalcoholic fatty liver disease. American Journal of Physiology-Gastrointestinal and Liver Physiology. 2021;320(3):G304-G18.

94.   Lin L-C, Quon T, Engberg S, Mackenzie AE, Tobin AB, Milligan G. G Protein-Coupled Receptor GPR35 Suppresses Lipid Accumulation in Hepatocytes. ACS Pharmacology & Translational Science. 2021;4(6):1835-48.

95.   Ma B, Zhu J, Tan J, Mao Y, Tang L, Shen C, et al. Gpr110 deficiency decelerates carcinogen-induced hepatocarcinogenesis via activation of the IL-6/STAT3 pathway. American journal of cancer research. 2017;7(3):433.

96.   Hagiwara M, Brindle P, Harootunian A, Armstrong R, Rivier J, Vale W, et al. Coupling of hormonal stimulation and transcription via the cyclic AMP-responsive factor CREB is rate limited by nuclear entry of protein kinase A. Molecular and cellular biology. 1993;13(8):4852-9.

97.   Kopec AK, Abrahams SR, Thornton S, Palumbo JS, Mullins ES, Divanovic S, et al. Thrombin promotes diet-induced obesity through fibrin-driven inflammation. The Journal of clinical investigation. 2017;127(8):3152-66.

98.   Rusli F, Deelen J, Andriyani E, Boekschoten MV, Lute C, van den Akker EB, et al. Fibroblast growth factor 21 reflects liver fat accumulation and dysregulation of signalling pathways in the liver of C57BL/6J mice. Scientific reports. 2016;6(1):1-16.

99.   Wree A, Broderick L, Canbay A, Hoffman HM, Feldstein AE. From NAFLD to NASH to cirrhosis—new insights into disease mechanisms. Nature reviews Gastroenterology & hepatology. 2013;10(11):627-36.

100.   Tilg H, Moschen AR. Evolution of inflammation in nonalcoholic fatty liver disease: the multiple parallel hits hypothesis. Hepatology. 2010;52(5):1836-46.

101.   Cao B, Liu C, Zhang Q, Dong Y. Maternal high-fat diet leads to non-alcoholic fatty liver disease through upregulating hepatic SCD1 expression in neonate rats. Frontiers in nutrition. 2020;7:581723.

102.   Gjorgjieva M, Sobolewski C, Dolicka D, de Sousa MC, Foti M. miRNAs and NAFLD: from pathophysiology to therapy. Gut. 2019;68(11):2065-79.

103.   Ntambi J. Dietary regulation of stearoyl-CoA desaturase 1 gene expression in mouse liver. Journal of Biological Chemistry. 1992;267(15):10925-30.

104.   Strable MS, Ntambi JM. Genetic control of de novo lipogenesis: role in diet-induced obesity. Critical reviews in biochemistry and molecular biology. 2010;45(3):199-214.

105.   Iizuka K, Horikawa Y. ChREBP: a glucose-activated transcription factor involved in the development of metabolic syndrome. Endocrine journal. 2008:0805150144-.

106.   Ferre P, Foufelle F. Hepatic steatosis: a role for de novo lipogenesis and the transcription factor SREBP-1c. Diabetes, obesity and metabolism. 2010;12:83-92.

107.   Ducheix S, Lobaccaro J, Martin P, Guillou H. Liver X Receptor: an oxysterol sensor and a major player in the control of lipogenesis. Chemistry and physics of lipids. 2011;164(6):500-14.

108.   Oballa RM, Belair L, Black WC, Bleasby K, Chan CC, Desroches C, et al. Development of a liver-targeted stearoyl-CoA desaturase (SCD) inhibitor (MK-8245) to establish a therapeutic window for the treatment of diabetes and dyslipidemia. Journal of medicinal chemistry. 2011;54(14):5082-96.

109.   Girardin Ml, Dolman SJ, Lauzon S, Ouellet SpG, Hughes G, Fernandez P, et al. Development of a practical synthesis of stearoyl-CoA desaturase (SCD1) inhibitor MK-8245. Organic Process Research & Development. 2011;15(5):1073-80.

110.   Cui H, Zhu X, Li S, Wang P, Fang J. Liver-targeted delivery of oligonucleotides with N-acetylgalactosamine conjugation. ACS omega. 2021;6(25):16259-65.

111.   Ducheix S, Piccinin E, Peres C, Garcia-Irigoyen O, Bertrand-Michel J, Fouache A, et al. Reduction in gut-derived MUFAs via intestinal stearoyl-CoA desaturase 1 deletion drives susceptibility to NAFLD and hepatocarcinoma. Hepatology Communications. 2022.

112.   MacDonald ML, Van Eck M, Hildebrand RB, Wong BW, Bissada N, Ruddle P, et al. Despite antiatherogenic metabolic characteristics, SCD1-deficient mice have increased inflammation and atherosclerosis. Arteriosclerosis, thrombosis, and vascular biology. 2009;29(3):341-7.

113.   Jiang G, Li Z, Liu F, Ellsworth K, Dallas-Yang Q, Wu M, et al. Prevention of obesity in mice by antisense oligonucleotide inhibitors of stearoyl-CoA desaturase–1. The Journal of clinical investigation. 2005;115(4):1030-8.

114.   Brown JM, Rudel LL. Stearoyl-coenzyme A desaturase 1 inhibition and the metabolic syndrome: considerations for future drug discovery. Current opinion in lipidology. 2010;21(3):192.

115.   Li ZZ, Berk M, McIntyre TM, Feldstein AE. Hepatic lipid partitioning and liver damage in nonalcoholic fatty liver disease: role of stearoyl-CoA desaturase. Journal of Biological Chemistry. 2009;284(9):5637-44.

116.   Liu J, Cinar R, Xiong K, Godlewski G, Jourdan T, Lin Y, et al. Monounsaturated fatty acids generated via stearoyl CoA desaturase-1 are endogenous inhibitors of fatty acid amide hydrolase. Proceedings of the National Academy of Sciences. 2013;110(47):18832-7.

117.   Cooper ME, Regnell SE. The hepatic cannabinoid 1 receptor as a modulator of hepatic energy state and food intake. British journal of clinical pharmacology. 2014;77(1):21-30.

118.   Zhu X, Huang G, Jin P. Clinicopathological and prognostic significance of aberrant G protein-couple receptor 110 (GPR110) expression in gastric cancer. Pathology-Research and Practice. 2019;215(3):539-45.

119.   Bhat RR, Yadav P, Sahay D, Bhargava DK, Creighton CJ, Yazdanfard S, et al. GPCRs profiling and identification of GPR110 as a potential new target in HER2+ breast cancer. Breast cancer research and treatment. 2018;170(2):279-92.

120.   Liu Z, Zhang G, Zhao C, Li J. Clinical significance of G protein-coupled receptor 110 (GPR110) as a novel prognostic biomarker in osteosarcoma. Medical Science Monitor: International Medical Journal of Experimental and Clinical Research. 2018;24:5216.

121.   Sadras T, Heatley SL, Kok CH, Dang P, Galbraith KM, McClure BJ, et al. Differential expression of MUC4, GPR110 and IL2RA defines two groups of CRLF2-rearranged acute lymphoblastic leukemia patients with distinct secondary lesions. Cancer Letters. 2017;408:92-101.

122.   Shi H, Zhang S. Expression and prognostic role of orphan receptor GPR110 in glioma. Biochemical and Biophysical Research Communications. 2017;491(2):349-54.

123.   Espinal-Enríquez J, Muñoz-Montero S, Imaz-Rosshandler I, Huerta-Verde A, Mejía C, Hernández-Lemus E. Genome-wide expression analysis suggests a crucial role of dysregulation of matrix metalloproteinases pathway in undifferentiated thyroid carcinoma. BMC genomics. 2015;16(1):1-23.

124.   Falvella FS, Pascale RM, Gariboldi M, Manenti G, De Miglio MR, Simile MM, et al. Stearoyl-CoA desaturase 1 (Scd1) gene overexpression is associated with genetic predisposition to hepatocarcinogenesis in mice and rats. Carcinogenesis. 2002;23(11):1933-6.